# Towards the mechanical activation of TMTACN-Cu based complexes

Tam, S.W.

*Award date:*
2015

# Towards the mechanical activation of TMTACN-Cu based complexes

Graduation report of

**S.W Tam**

Molecular Engineering Master Program

Eindhoven University of Technology

# Towards the mechanical activation of TMTACN-Cu based complexes

**Graduation report of**

S.W. Tam

**Supervisor**

dr. E. Schwartz

**Supervising professor**

Prof. dr. R.P Sijbesma

**Advising committee**

dr. E.A. Pidko

**June 2014**

**Laboratory Molecular Science and Technology**

**Department of Chemical Engineering and Chemistry**

**Eindhoven University of Technology**

## Summary

Chemical reactions are commonly initiated by absorption of an energy trigger that can be achieved by different energy sources, such as light, heat or electricity. An alternative way to induce a reaction is by direct absorption of mechanical energy, generally referred to mechanochemistry. Besides the incorporation of mechanophores in polymers to trigger certain events by mechanical force, a similar concept can also be used to activate latent catalysts. In mechanocatalysis, a dormant catalyst is activated under mechanical force. A dormant catalyst is in a 'sleeping' state, where the catalyst is inactive.

In this project we investigated the mechanical activation of a 1,4,7-trimethyl-1,4,7-triazacyclononane (TMTACN)-copper(II) based catalyst. The dimeric copper complex is inactive towards the hydrolysis reaction of phosphate esters, while the mononuclear diaqua copper complex, which is in equilibrium with the dormant binuclear form, is able to hydrolyze phosphate esters. Therefore, we envisioned that by incorporation of the inactive dimeric complex in a polymeric network, activity may be achieved upon application of mechanical force, because the binuclear structure will be transformed into the active mononuclear complex.

After an introduction on mechanochemistry, in chapter 2, the synthetic strategies and the design towards the mechanocatalyst are described. From the strategies explored, it was found that in order to incorporate the catalyst into a polymer network, a ligand functionalized with a polymerizable group should be synthesized. And moreover, the dimeric copper structure should be stabilized, which can be done by bridging the two copper centers with an oxalate anion. The successful synthesis of the polymerizable ligand and the formation of the dimeric oxalate bridged copper complex with this ligand are reported in chapter 2 and 3, respectively.

In chapter 3, the synthesis of related complexes based on the TMTACN ligand and their use in the hydrolysis of *p*-nitrophenylacetate (*p*NPA) and bis(*p*-nitrophenyl)phosphate (BNPP) are discussed. As outlined in chapter 4, it was found that the mononuclear diaqua complex is active in the hydrolysis reaction of both substrates, whereas the oxalate bridged dimeric complex showed activity in dilute solutions and no activity at high concentrations, for the *p*NPA and BNPP hydrolysis, respectively. It suggests that a substantial amount of the dimeric complex dissociates into mononuclear species in dilute solutions.

In chapter 5, force studies on copper oxalate complex with the polymerizable ligand, which was incorporated in a poly(2-hydroxyethylmethacrylate) (pHEMA) network, are reported. This polymer film was swollen in a buffered BNPP solution at 50 °C. Catalytic activity of the polymer films with the copper oxalate complex was observed. However, further studies should be carried out in order to correlate the solvent swelling with the observed activity in hydrolysis.

## Table of Contents

# Chapter 1 Introduction

Chemical reactions are commonly initiated by absorption of an energy trigger that can be achieved by different energy sources, such as light, heat or electricity. An alternative way to induce a reaction is by direct absorption of mechanical energy, generally referred to mechanochemistry.[1]
Mechanochemical reactions can be found in the milling or grinding of crystals, metals and alloys, for example $Si_3N_4$ can be synthesized upon milling of silicon in $NH_3$ and $N_2$ atmospheres.[2–4] Examples of mechanical stimulated processes can also be found in nature; for example the clotting of blood by platelet formation is regulated by the release of the corresponding factor due to the conformational change of a protein originated from elongational stress that occur when blood flows to the hemorrhage.[5]

## 1.1 Fundamental aspects of polymer mechanochemistry

Mechanically stimulated processes also can be found in synthetic materials, as already reported in the 1930s by Herman Staudinger. He observed a decrease of polymeric weight upon mastication[6], and attributed this decrease to the mechanical rupture of polymers. In the 1940s, Kauzmann and Eyring developed the Thermal Activation to Bond Scission (TABS) theory[7]; it explains that for a covalent bond under force, the corresponding Morse energy potential will be altered as compared to an unstretched covalent bond (Figure 1.1). It, moreover, results in the lowering of the bond dissociation energy, and when this dissociation energy is lowered enough, the thermal fluctuations ($k_bT$) can overcome this barrier to cause chemical bond rupture.

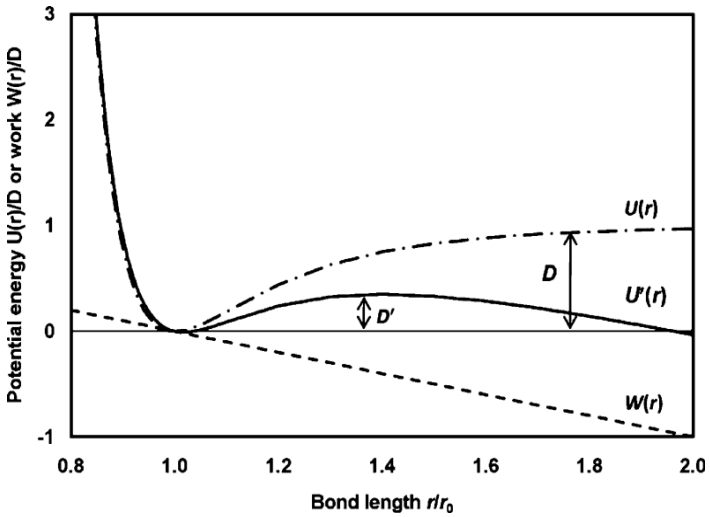


**Figure 1.1 Under external force, given by the work potential (*W(r)*), the resulting Morse potential of a covalent bond will be altered (*U'(r) = U(r) - W(r)*), to give rise to a lowered activation barrier for bond dissociation (*D'*).**

Another fundamental aspect in polymer mechanochemistry is the transduction of applied force towards the actual bond breaking process. Earlier work on polymer degradation in solutions showed that elongational flow field generates strong hydrodynamic forces on a polymer chain. The polymer

chain unfolds and elongates, due to strain imposed by the external force. Eventually, chain scission occurs when the critical strain rate is reached.[8,9] It was found that by increasing the molecular weight, the critical strain rate decreased. This observation could be later on confirmed by the bead-rod model,[8–10] which describes that force accumulated on an extended polymer chain scales with its molecular weight, $F_{max} \sim M^2$. This relation also suggests that chain scission can only be achieved when the molecular weight is sufficient to build up the force along the backbone; there is a limiting molecular weight ($M_{lim}$) to induce mechanical rupture.[10–15] Typical limiting molecular weights for covalent polymers are estimated at 40- 100 kg $mol^{-1}$. [16] It can also be deduced that mechanical scission is a non-random process, and that it occurs predominantly at the center of the polymer chain, because the accumulated force will be maximal at the mid-point. [10–14]

A reaction that is mechanically induced can alter the reaction pathway. This was demonstrated by different products obtained in the ring-opening reaction of cyclobutanes (CB) under mechanical activation and by thermal activation. The formation of different products could be rationalized by a lowered energy barrier for a certain pathway due to the involvement of anisotropy (directionality) in applied force (Figure 1.2).[17,18] It means that for a mechanically induced reaction, change in the energy landscape can be found, and therefore the reaction pathway for such reactions will be different compared to their thermal or photo-chemical stimulated analogues.

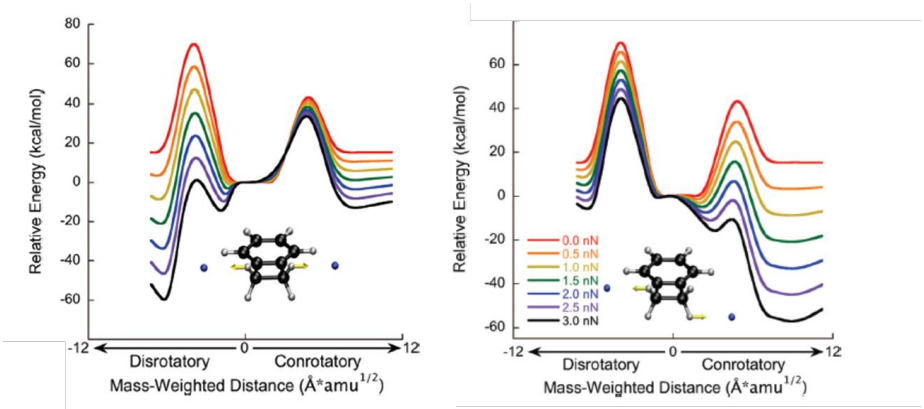


**Figure 1.2 Modified energy landscape of cis- and trans-substituted CB upon application of force.**

## 1.2 Methods and techniques for mechanical activation

As the field of polymer mechanochemistry is matured, techniques to perform mechanical transduction were also developed. Depending on the polymer state, that is in solution or in bulk, a variety of techniques can be applied to generate forces and strain rates (Figure 1.3).[19] In general, the force applied should exceed ~$10^{-10}$ N to cause a single bond scission. For solvated polymers high strain rates of $10^4$ $s^{-1}$ are necessary to promote molecular deformation that will be faster than molecular vibration.[19]

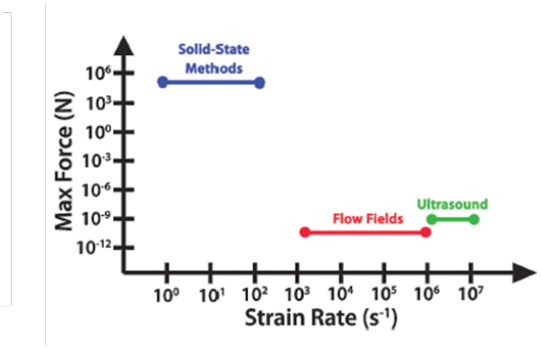


**Figure 1.3 Schematic overview of experimental methods to generate mechanical activation on a material.**

### 1.2.1 Mechanical activation in solid state

Solid state methods can reach up to $10^5$ N in applied force, but relatively low strain rates are generated (Figure 1.3).[20] A simple method to perform elongational force on a polymer material is by manual stretching. Although the force and strain rates can not be quantified, the mechanical activation of the material can be qualitatively tested.[20]

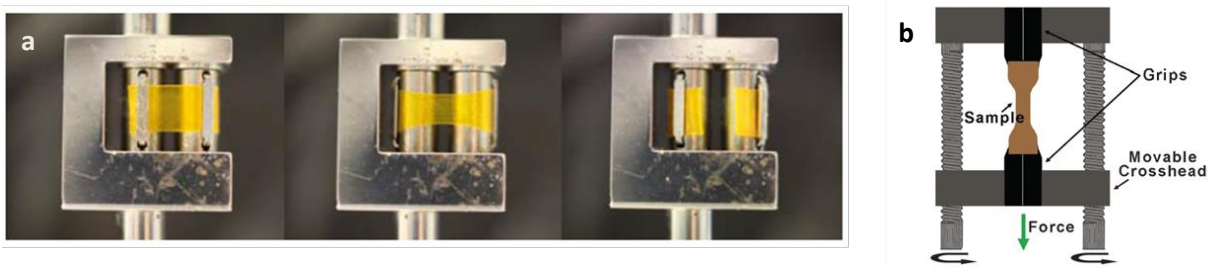


**Figure 1.4 (a) elongational forces on polymer material can be applied, by rotation of the drums with attachment of polymeric material in opposite fashion. (b) Upon movement of the screws, forces exert on the molded polymer, which is fixated at the movable crosshead.**

Rheometers equipped with an extensional fixture are able to stretch uniform molded polymer films in a controlled and quantified manner. Force generation on polymeric material with strain rates up to 8 $s^{-1}$ is achieved by rotation of drums with polymer film attached (Figure 1.4).[21] Another tensile testing instrument that exerts force in controlled manner is a screw-driven load frame. Elongational deformations are created upon stretching the polymer, which is molded in a dog bone shape fixated between two wedge grips (Figure 4).[22]

Opposite to elongational forces, stress into a material can be induced by compressional forces. The force (F) applied under compression is related to the pressure (P) applied on a sample with a known area (A), by the relation $P = F \times A^{-1}$. Many different apparatuses are known to apply compressional forces, such as a steel piston[23] or a diamond anvil press.[24] A comparatively more simple method, is by using hydraulic presses, as this equipment is often readily available in a laboratory for making KBr pellets that can be used for IR spectroscopy.

### 1.2.2 Mechanical activation in solution

As alluded above, high strain rates for solvated polymers are required to induce a molecular deformation. The high strain rates can be generated by flow fields and ultrasound irradiation (Figure 1.3).[19] In previous studies, a variety of flow devices have been used to study polymer degradation in flow fields.[19] Such an equipment can be a cross slot device that create a flow field through opposing orifices (Figure 1.5).[25] The flow field contains a region where the velocity is zero, i.e. the stagnation point. And for a polymer chain that is trapped in this region experiences a high velocity gradient in its vicinity. This result in elongatation and eventually rupture of a polymer chain.

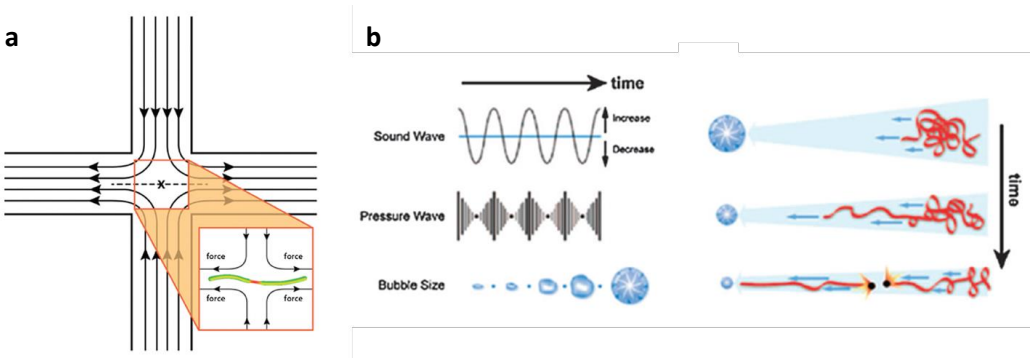


**Figure 1.5 (a) Diagram of elongational flow created by a cross-slot device; at the stagnation point a polymer chain experience a high velocity gradient, and thereby inducing chain rupture (b) Schematic overview of the formation of nucleation bubbles by the acoustic and pressure waves passing though liquid. Unfolding, elongation and eventually breaking of a polymer chain, results from the hydrodynamic force field created upon implosion of the cavitation bubble.**

Another method to generate force on a polymer in solution is by means of ultrasound irradiation. The low frequency (> 20 kHz) acoustic sound waves from ultrasound irradiation compress and expand fluid that leads to cavitation bubble formation. The growth of this bubble is achieved through nucleation around gas bubbles dissolved in solution.[26] At certain point this bubble will collapse, and the inwards motion of the collapsing bubble generates high velocity gradients and strain rates in its vicinity.[27,28] A hydrodynamic force field emerged from the high velocity gradient causes as a polymer chain near the imploding bubble to unfold, stretch and break (Figure 1.5). [27–29]

### 1.3 Mechanoresponsive materials

In recent years, research in polymer science has shifted towards the development of smart materials, in which properties can be tuned in a controlled manner by applying external stimuli. Mechanoreponsive materials are materials, which under mechanical force give rise to a response that can be chromism, lumiscence, catalysis or self-healing properties. Incorporation of a weak bond

in a polymer chain that, under application of force can undergo a useful reaction, is essential in the design of such materials.[30,26,20,17]

There are multiple examples of mechanically induced responsive materials mediated by non-covalent interactions reported.[31–35] A recent example was shown by Azzaroni et al.; a large color shift was observed upon compression of immobilized poly[(2-methacroyloxy)ethyl]trimethylammonium chloride on glass with bromothymol blue dye interspersed. This is a result from the increased interaction of the pH sensitive dye and the strong polyelectrolytic brush. A covalent alternative of a mechanochromic material developed by Davis et al. showed that by incorporation of a spiropyran moiety in glassy and elastomeric polymers, the covalent spiro C – O bond can be broken under tensile stress, leading to a large color shift by the formation of merocyanine (Figure 6).[36] Inspired by this work, our group has developed a material containing crosslinked bis-ademantyl- 1,2-dioxetane unit, that can undergo electrocyclic ring opening to yield two ketones. One ketone is in the excited state, and will emit light upon relaxation to the ground state (Figure 1.6). [21]

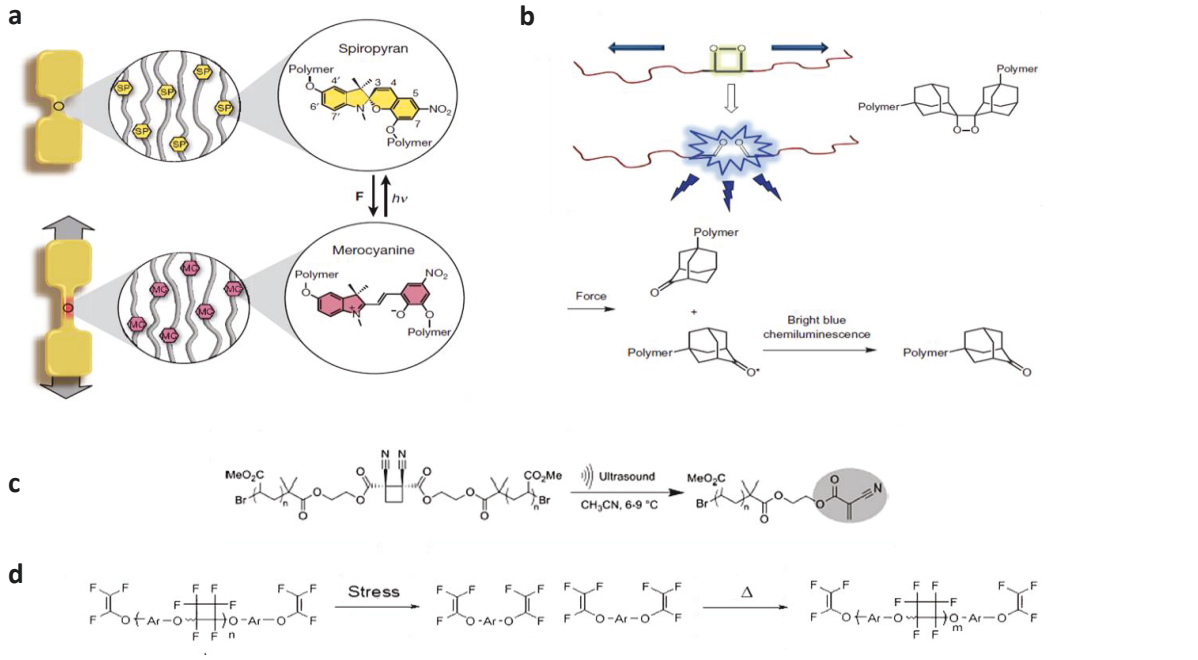


**Figure 1.6 Examples of mechanochemistry in polymeric materials (a) Upon incorporation of a spiropyran moiety in a polymer, mechanically induced ring opening of a spiropyran to the red merocyanine dye is observed. (b) Tensile stress applied on a bis-ademantyl-1,2-dioxetane functionalized network leads to formation an excited ketone and upon relaxation of this, emission of light is observed. (c) Upon ultrasound irradiation of dicyanocyclobutane incorporated polymers leads to formation of highly reactive cyano-acrylate end groups. (d) Self-healing properties can be found in degradation and regeneration of perfluorocyclobutane polymer upon stress and heating applied, respectively.**

Other mechanoresponsive materials developed for application purposes are self-healing materials. Polymers are in general susceptible towards mechanical damage.[37] Self-healing materials make use of this phenomenon by enhancement of strength or toughness when
failure of material seems to manifest.[38,39] Self-healing properties can be achieved by incorporating both encapsulated dicyclopentadiene (DCPD) monomers and Grubb's catalyst in an epoxy matrix. Mechanical damage results in crack formation that releases the encapsulated DCPD. The released DCPD that is in contact with the catalyst will perform ring opening metathesis reaction (ROMP).[38] A molecular approach to this was explored in Moore's group. It was shown that upon ultrasound irradiation of incorporated dicyano-cyclobutane moieties in polymers, resulted in the ring opening of the cyclobutane to yield highly reactive cyanoacrylate end groups (Figure 1.6).[40] Craig et al. have developed a polymer that consists of perfluorocyclobutane units, which under ultrasound irradiation depolymerizes into trifluorovinyl ether fragments.[41] Upon heating of these fragments, the polymer is reformed, although with a lower molecular weight as compared to the initial polymer. This example shows the potential of polymer mechanochemistry to construct self-healing materials, though it is still far from the ideal, autonomous, self-healing material. For which the repair mechanism will be only by a mechanical trigger, thus without any external stimuli, such as heating.

### 1.3.1 Mechanocatalysis

Besides the incorporation of mechanophores in polymers to trigger certain events by mechanical force, a similar concept can also be used to activate latent catalysts. In mechanocatalysis, these latent or dormant catalysts are in 'sleeping' state before mechanical force is applied, and (ideally) will be activated upon applying a mechanical force.

Previous studies from our group have shown reversibility in bond breaking processes of coordination polymers upon ultrasound irradiation.[42–44] It was observed that a phosphane derived polymer remained unbroken and that only the weaker metal-phosphine bond was mechanically activated. These results showed the possibilities of value in mechanocatalysis, as selective ligand dissociation is obtained upon mechanical activation of the transition metal - ligand complex. Inspired by this work, the development of N-heterocyclic carbene (NHC) functionalized polymers coordinated to silver(I), which under sonication dissociates to generate a (free) carbene, have been constructed. [45] The carbene acts as a catalyst in the catalytic transesterification reaction of benzyl alcohol and vinyl acetate. The metal can also catalyze a reaction under these conditions, as could be seen by the bis-NHC ruthenium complex. This mechanically activated ruthenium complex is active in the ring closing metathesis of diethyl adiallylmalonate (DEDAM) (Figure 1.7).[45] A mechanocatalyst that combines organo- and metal catalysis was developed in the group of Bielawski. [46] The catalyst consists of a dipalladium complex that is coordinated to a polymer derived pyridine. Upon sonication pyridine is liberated, which acts as an active catalyst for the anionic polymerization of highly electron deficient α-trifluoromethyl -2, 2, 2 -trifluoroethyl acrylate. Concomitantly, the Pd-metal catalyzes carbon-carbon bond formation of benzylcyanide and N-tosyl imines (Figure 1.7).

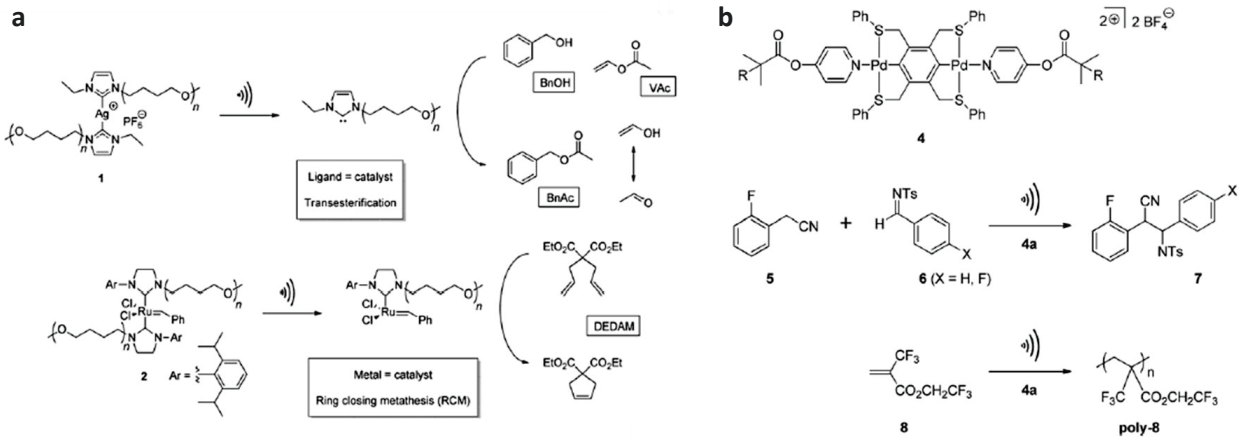


**Figure 1.7 Examples of mechanocatalysis (a) transesterfication and ring opening metathesis reaction catalyzed by silver and ruthenium NHC based complexes, respectively (b) C-C bond formation between *N*-tosyl imines catalyzed by Pd-complex and polymer derived pyridine catalyzes anionic polymerizations of trifluoroethyl acrylate moiety.**

Previous examples mentioned above involve homogeneous mechanocatalysis in solution; mechanical activation of solid material is less explored yet. Moore and co-workers developed a system based on gem-dichlorocyclopropanated indene which upon mechanical activation led to the elimination of HCl.[47] The generation of acid was confirmed by the color change into pink of the methyl red indicator. In our group, mechanical activation of a catalyst in solid state was also explored. Incorporation of a bis-NHC ruthenium complex in a semi-crystalline network showed activation towards ring opening metathesis polymerization of a nobornene monomer upon compression of the material.[48]

## 1.4 Trimethyltriazacyclononane (TMTACN) – copper catalyst

Nature has always inspired scientists to develop systems to mimic biological processes. Often high efficiencies can be reached for such processes. Phosphate ester hydrolysis is such a process; it proceeds by a large rate enhancement in a biological environment. Phosphodiester bonds play important roles in nature, as these can be found in the stable backbone of deoxyribonucleic acid (DNA) and ribonucleic acid (RNA). It has been proven that the half-life of phosphoester bonds in DNA is estimated at 130 000 years at near physiological conditions.[49] Apart from being present in genetic material, it can be also found in phospholipids, organic cofactors (ATP, coenzyme A, FAD, $NAD^+$) and secondary messengers (cAMP, cGMP, $IP_3$).[50] Although these phosphate ester bonds are very stable, dephosphorylation (and also phosphorylation) is essential in intracellular signalling, DNA repair, RNA maturation, energy storage and production.[50] Therefore nature has developed enzymes that facilitate hydrolysis of P-O bonds with an acceleration of a factor $10^{15}$.[51] (Scheme 1.1) The tremendous rate enhancement observed by these enzymatic machineries have lead to the development of small molecule synthetic mimics. Development of these synthetic mimics have led

to a better understanding in the mechanism of action. In addition, it can also be used to create new biotechnological tools and nucleic acid-targeting therapeutics.[52–54]

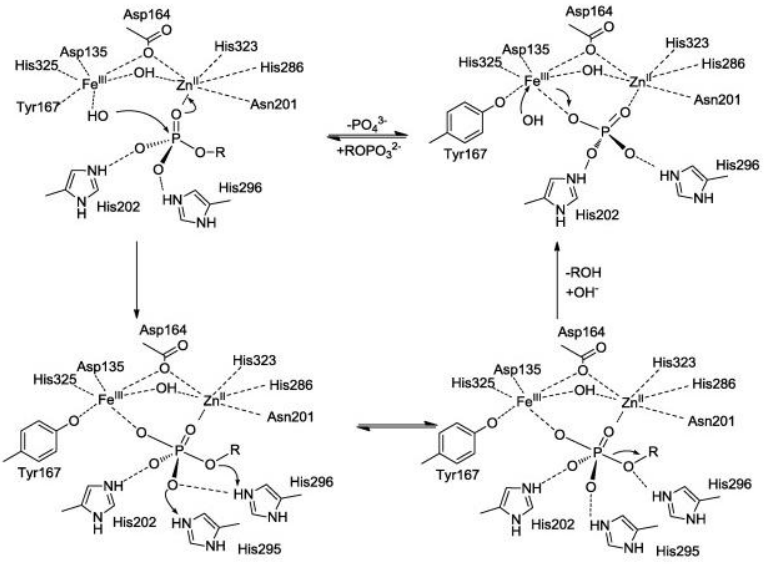


**Scheme 1.1 Proposed catalytic cycles for kidney bean purple acid phosphatase (PAP).** [55]

### 1.4.1 Development of small molecule mimics based on Cu(II), Zn(II) and Ni(II) based complexes

The development of synthetic mimics was initiated by the finding of Wacker and co-workers, that $Cu^{2+}$, $Cr^{2+}$, $Fe^{3+}$, $Ni^{2+}$, $Mg^{2+}$, $Ca^{2+}$ , $Pb^{2+}$ ions can hydrolyze the phosphoester bond in Tobacco Mosaic Virus RNA at 65 °C.[56] In the 1980s, a phosphate monoester was incorporated into a 1,2-diaminoethane (en) chelating cobalt $[Co(en)_2(OH)O_3POC_6H_4NO_2]$ complex.[57] By $^{18}O$-labeling of the coordinated hydroxide a pathway was proposed, in which the phosphate ester bond is cleaved by intramolecular attack of the hydroxide. The proposed mechanism involves the formation of a trigonal bipyramidal coordinated phosphorane, which upon hydrolysis nitrophenol is released. Moore and Trogler showed catalytic activity in DNA model system by a Cu(II) 2,2-bipyridine (bpy) complex.[58] Follow up studies on the size effect of the chelating ligand were perfomed, by comparing bpy ligand with tris(2-aminoethyl) amine (tren) ligand complexed with Cu(II), Zn(II) and Ni(II) - metal ions.[59] It showed that the Cu(II)-bpy complex achieved the highest activity. This can be explained by the smaller bpy ligand, which allows coordination of substrate and the OH nucleophile simultaneously, leading to the formation of a pre-transition state. Compared to the larger tren ligand complexes, binding of both is prohibited, and therefore, a decrease in activity is observed. Kimura and Koike have showed that triazacyclododecane ([12]ane$N_3$) are also compatible ligands in phosphate ester hydrolysis, as the complex with Zn(II) also facilitated both binding of substrate and nucleophile.[60]

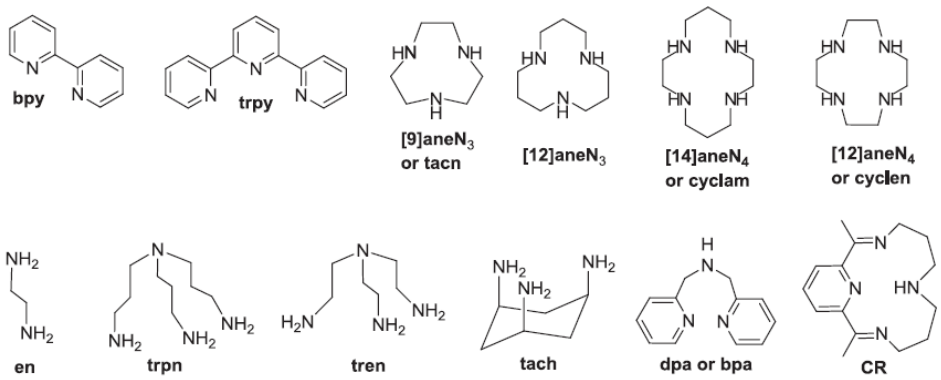


**Figure 1.8 A few examples of chelating ligands that were used in the studies towards small molecule mimics in phosphate ester hydrolysis.**

### 1.4.2 1,4,7-trimethyltriazacyclononane – Cu(II) complexes in phosphate ester hydrolysis

In the 1990s, the group of Burstyn developed a tridentate chelating ligand, 1,4,7-triazacyclononane (tacn), coordinated to Cu(II) complex.[61] They found that the mononuclear $[(tacn]Cu(OH)(OH_2)]^{2+}$ complex act as the active species in the catalytic cycle, and moreover, is in equilibrium with the inactive dimeric $[(tacn)_2Cu_2(\mu\text{-}OH)_2]^{2+}$ complex. This dimeric complex is favored at neutral pH, with a dimerization constant ($K_{dim}$) of 1220 $M^{-1}$ .[62–64] Substituting bulkier groups on the amine of the macrocycle lead to a decrease of dimerization towards the binuclear structure, as the N – alkylated triisopropyl and trimethyl-1,4,7-triazacyclononane ligand show rate enhancement by a factor of 50 and 200 as compared to the unsubstituted analogues, respectively.[65,66] The group of Brügger have proposed a mechanism towards BNPP hydrolysis [66] (Figure 1.9); the catalytic cycle proceeds by dissociation of the dimeric copper complex that results in the active mononuclear complex. Coordination of bis-(4-nitrophenyl) phosphate (BNPP) substrate by ligand exchange of the coordinated water, results in the polarization of the P-O bond by the lewis acidic copper center. This facilitates intramolecular attack from the hydroxide nucleophile on the phosphate ester to yield the hydrolyzed product. And finally, after ligand exchange of water with the hydrolyzed product, the catalyst is obtained after protonation of the water.

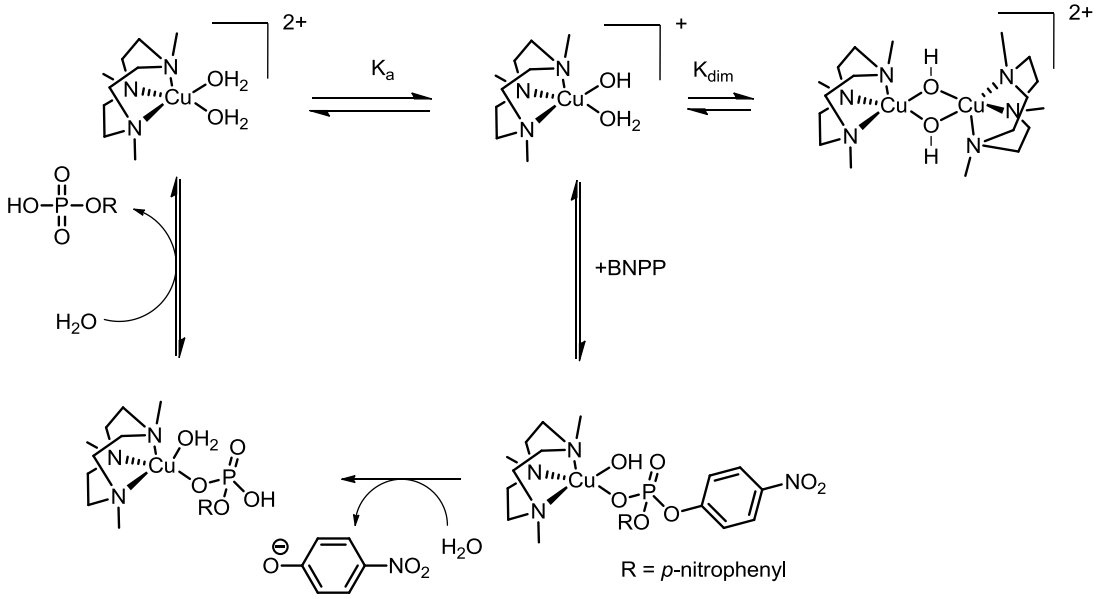


**Figure 1.9 Catalytic cycle of TMTACN=Cu based complex in BNPP hydrolysis proposed by Brügger et al.**

## 1.5 Aim and outline of project

To broaden the scope of mechanocatalysts we aim to study the mechanical activation of Cu-TMTACN complexes that can catalyze the hydrolysis of BNPP. We envision that, when the inactive dimeric complex is incorporated in a polymeric network, catalytic activity may be induced upon application of mechanical force. In chapter 2, different strategies towards the mechanocatalyst are investigated and the synthesis and characterization towards the polymerizable TMTACN derivative is reported. Upon the successful synthesis of the polymerizable ligand, its complexation with copper(II) is investigated in chapter 3. Moreover in this chapter, TMTACN based copper complexes needed to study the hydrolysis of model substrates, prior to the mechanical activation of a mechanocatalysta re discussed in in chapter 4, which the activity towards bis(*p*-nitrophenyl)phosphate (BNPP) and *p*-nitrophenylacetate (*p*NPA) hydrolysis with the model TMTACN-copper(II) system is examined.
And finally, upon incorporation of the polymerizable copper complex in a poly(2-hydroxyethylmethacrylate) (pHEMA) network, the mechanically induced catalytic activity of the polymer films by solvent swelling is studied in Chapter 5.

# Chapter 2 Synthetic strategies towards the design of TMTACN-Cu based mechanocatalysts

## 2.1 Exploration of different strategies

To meet the requirements for a mechanocatalyst to function properly 1) a stable dormant catalyst is needed before it is activated by a mechanical force (2.1.1) and 2) the catalyst needs to be attached to a polymer in order to transduce macroscopic forces to metal-ligand bonds (2.1.2).

### 2.1.1 Investigation of (inactive) dimeric structures

To ensure inactivity prior to mechanical activation of the mechanocatalyst, a stable dormant species is required. As outlined in paragraph 1.4.2, the TMTACN copper complex is in equilibrium with its active monomeric and inactive dimeric state. Although the equilibrium is shifted towards the binuclear complex, with a dimerization constant ($K_{dim}$) of 3020 $M^{-1}$, in dilute solution there will be a substantial amount of active mononuclear complexes present.[66] The dimeric structure can be stabilized by bridging the two copper centers with an anion. Various binuclear copper TMTACN complexes have been reported (Figure 2.1).[67] Most studies on these complexes are related to the determination of the magnetic exchange interactions between the two copper ions. The structural stability in water and the catalytic activity is often not reported. However, Deal and Burstyn showed that upon addition of oxalate to a solution containing an active complex copper and substrate (bis(*p*-nitrophenyl)phosphate) complete inhibition of hydrolysis was achieved.[62] It is plausible that a binuclear oxalate bridged complex was formed, which would be inactive in phosphate ester hydrolysis.

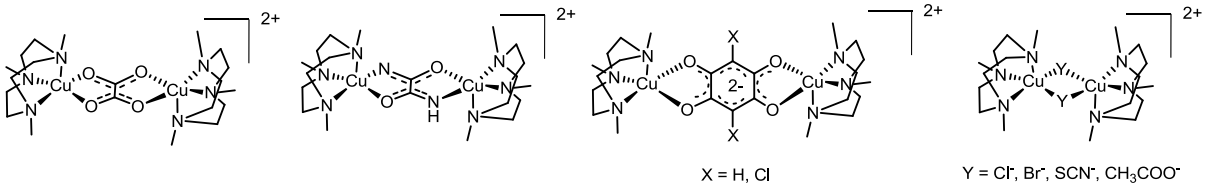


**Figure 2.1 Dinuclear copper complexes bridged with various kinds of anions.**

### 2.1.2 Investigation on different polymeric systems

In order to incorporate the TMTACN ligand in a polymer, a functionalizable TMTACN derivative should be synthesized. Considering the different polymers that can be used, two strategies can be envisioned; (i) a growing polymer chain that can be terminated upon addition of a functional end capping agent or (ii) a TMTACN derivative with a polymerizable end group that can be incorporated in a polymer by copolymerization with a monomer of choice (Figure 2.2).

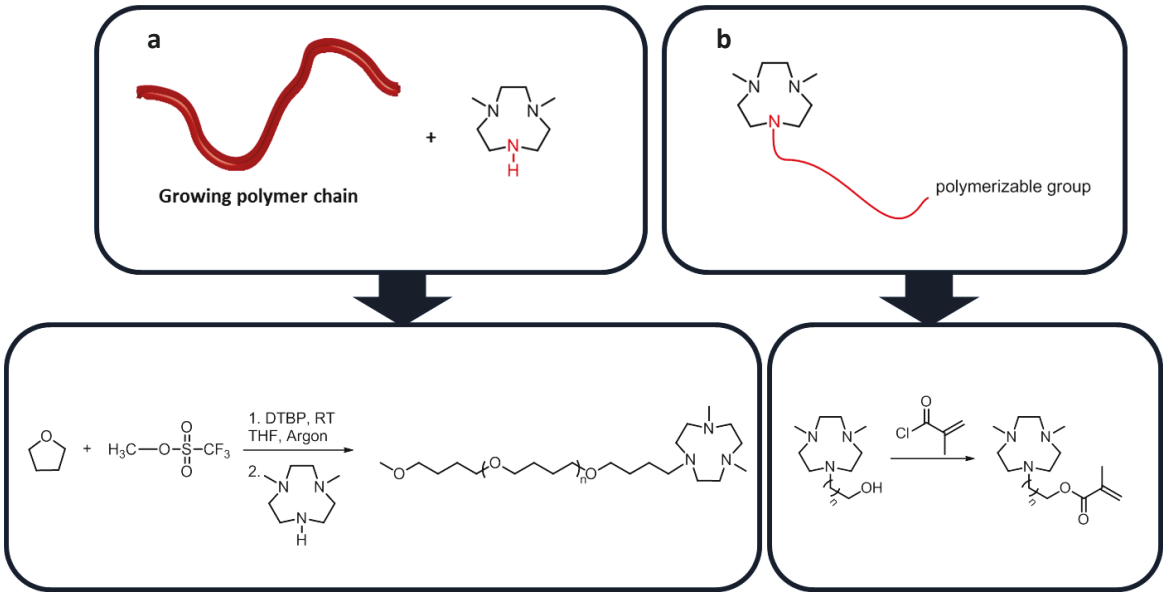


**Figure 2.2 Schematic overview of the strategies that can be employed to synthesize a (Cu-)TMTACN mechanocatalyst; (a) upon termination of a polymer chain with an end capping agent, a ligand derived polymer is obtained, (b) functionalization of the ligand with a polymerizable end group that can be incorporated in a polymer.**

Polytetrahydrofuran (pTHF) obtained by cationic ring opening polymerization of THF is commonly used in our group to obtain various mechanocatalysts. For this strategy a mono-functionalizable TMTACN derivative is required to terminate the living pTHF by end capping (Figure 2.2). Utilizing pTHF has its advantage in the narrow distribution of molecular weight (PDI < 1.4), while its molecular weight can be controlled according to the initiator concentration and reaction time.[16] Considering that water is needed to perform our catalytic reaction of choice, the hydrolysis of phosphate esters, the use of pTHF seems a less appropriate choice of polymer. Due to its (i) insolubility in water and (ii) effectiveness of polymer degradation by ultrasound irradiation in solvents with a high vapor pressure (i.e. water). The latter may be due to vapor entering the imploding cavitation bubble, leading to damping effects, and therefore, the resulting shear forces on polymer chains will be reduced.[10,68–70]

The second approach requires a TMTACN derivative with a functional handle already incorporated, to which a polymerizable group, for example a methacroyl moiety, can be attached. The spacer length can be easily tuned in this way, but should be of sufficient length to prevent coordination of the pendant arm to the copper center. Treating the polymerizable ligand with copper(II) and oxalate anion, will hopefully then lead to stable dimeric complexes that can act as a crosslinker in a polymeric network (Scheme 2.1).

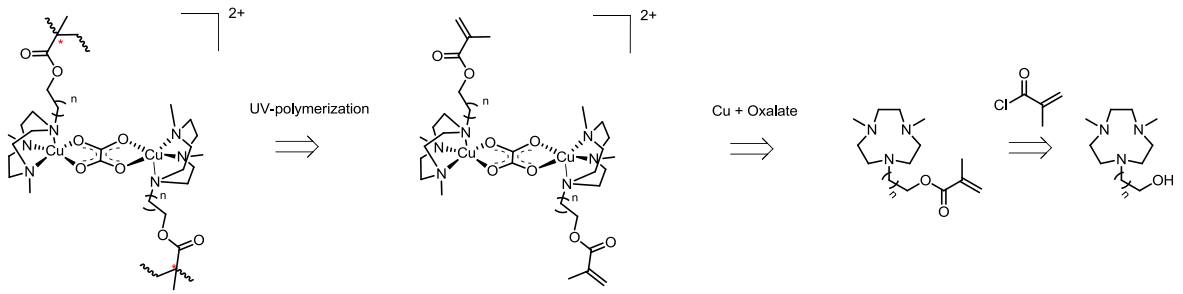


**Scheme 2.1 Retrosynthetic scheme of TMTACN-Cu incorporated polymer network. Fomation of a polymerizable TACN-ligand and upon condensation of the hydroxo pendant arm with methacryloyl chloride , the polymerizable ligand can be complexated with copper and incorporated in a polymeric network.**

## 2.2 Introduction

### 2.2.1 TACN and TMTACN macrocycles

The first synthesis of a TACN derivative was reported by Peacock and Gwan in 1937. By heating *N, N'*-di-*p*-toluenesulfonyl-*N, N'*-bis-(2-chloroethyl)ethylediamine with aqueous ammonia, the hydrochloride salt of a ditosylated triazacyclononane was obtained as a byproduct (Scheme 2.2).[71]

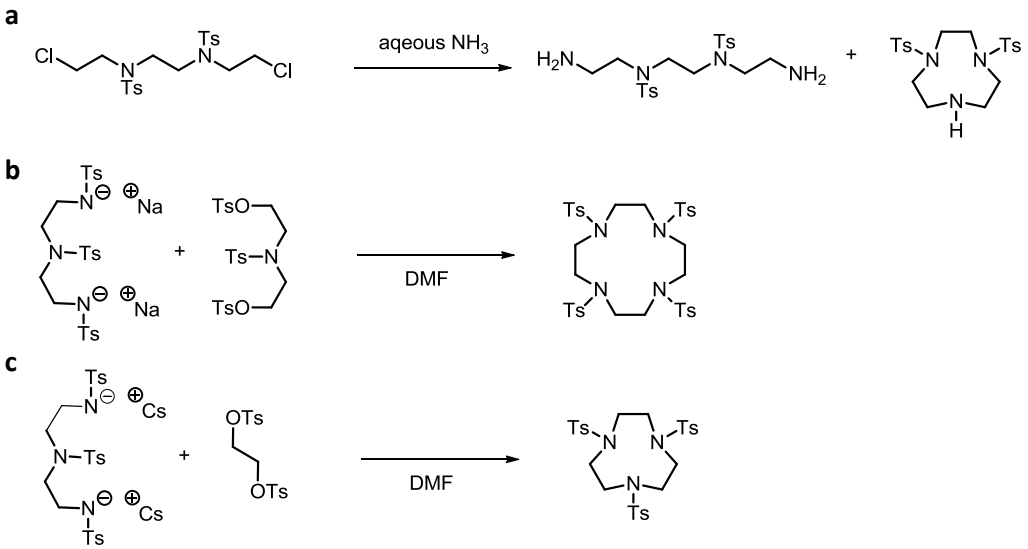


**Scheme 2.2 Synthesis of macroazacycles (a) Cyclization via nucleophilic attack of ammonia followed by ring closure to give to the ditosylated-TACN. (b,c) Treating a sulfonate ester with bisulfonamide salts leads to ring formation.**

Later, other cyclization methods were reported by Stetter, where the formation of macrocycles employs a high dilution technique of terminal halides and bissulfonamide sodium salts.[72,73] In general, dilution of the compounds favors the intramolecular ring closing process over intermolecular addition, which the rate of a ring closing process is proportional to the ring closing precursor concentration as for the intermolecular addition that leads to linear products, depends on the

square of the concentrations. In 1974, Richman and Atkins showed that the high dilution method could be improved. They used a bisulfonamide salt that yields tetrazacyclododecane (cyclen) macrocycles upon nucleophilic addition of the amine to leave the sulfonate ester in dipolar aprotic solvents.[74] Following the same principle, tritosylated TACN moieties can be obtained by treating bisulfonamide sodium salt with tosylated ethylene glycol. Vriesema et al. showed that with cesium tosylamides these cycles are also formed (Scheme 2.2). [75]

To yield the fully deprotected TACN, sulfonamide bonds can be cleaved by different methods, such as treating with strong acidic reagents, sodium or lithium metal in liquid ammonia, sodium amalgam, and sodium naphthalenide.[76] The trimethyl-1,4,7-triazacyclononane ligand which is most often used in catalysis, can be obtained by methylation via the Eschweiler-Clarke reaction, that is by treatment of TACN with formaldehyde and formic acid.[77]

### 2.2.2 Selective functionalization on TMTACN derivative – towards the incorporation of polymerizable end group

In recent years, selective functionalization of TACN became of interest due to the variety of donor-ligand types that can be obtained. Moreover, these variations may lead to different geometries of metal-ligand coordinations. Weisman et al. showed that treating TACN with *N,N*-dimethylformamide dimethyl acetal resulted in a tertiary orthoamide formation that can be hydrolyzed yielding a mono-formylated TACN (Scheme 2.3).[78] This can be protected twice using *p*-toluenesulfonylchloride (TsCl); subsequent hydrolytic removal of the formyl group was performed to yield the ditosylated TACN. Another approach to obtain a mono-functionalizable ligand was reported by the group of Sessler. Detosylation of the triprotected TACN, by heating up in 30% HBr in AcOH during a period of 36 h, gave rise to monotosylated TACN.[79] In more recent studies, substitution on TACN was successfully demonstrated by Brechbiel et al., who incorporated a functional handle directly into the ring. This was achieved via cyclization of *N, N*'-ditosylated protected disulfonate ester with a corresponding primary amine in the presence of sodium carbonate.[80] (Scheme 2.3)

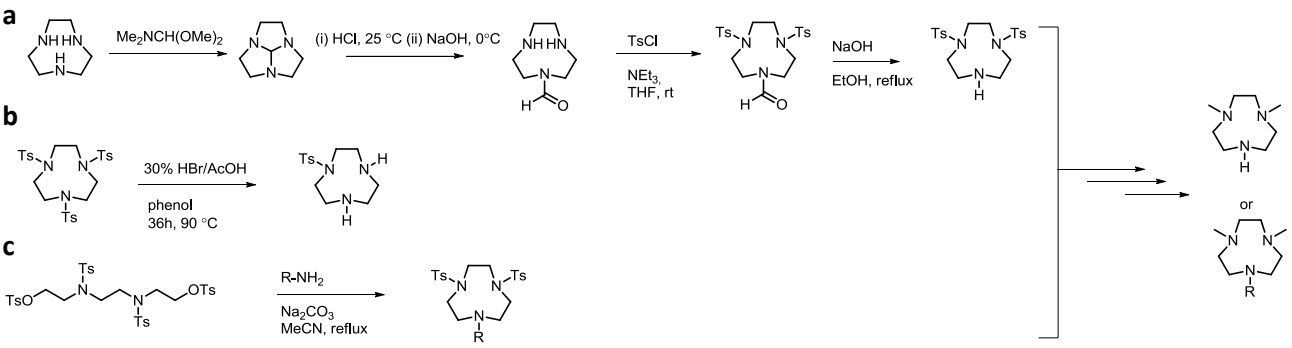


**Scheme 2.3 (a) Synthesis of tertiary orthoamide that can be hydrolyzed to obtain a mono *N*-formylated TACN, subsequent tosylation and formyl removal leads to monofuntionalizable TACN (b) detosylation in HBr/AcOH leads to the formation of monotosylated TACN (c) direct incorporation of a functional handle into the ligand is obtained by treating a disulfonate ester with a primary amine.**

In our project, further modification by reaction of the functional group of the pendent arm (i.e. –OH, $-NH_2$, $-N_3$) is desired (Scheme 2.4). In literature several procedures of efficient substitution of the amine are reported, mostly involving reactive species such as, epoxides and benzylhalides.[81,82] Reaction of the amine with an alkylhalide derivative was also reported, but requires the addition of an excess of the functionalizable 1,4-dimethyl-1,4,7-triazacyclononane during the reaction; this suggests that the amine is not very reactive in the substitution with an alkylhalide. [83]

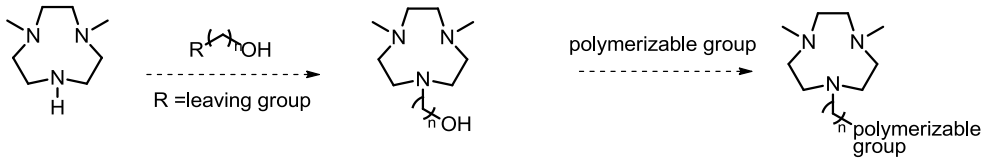


**Scheme 2.4 Proposed synthesis towards a polymerizable ligand.**

## 2.3 Results and discussion: synthesis of a mono-functionalizable TMTACN derivative, 1,4-dimethyl-1,4,7-triazacyclononane ($M_2$-TACN)

The synthetic route towards the desired TMTACN-derived ligand **6** is depicted in Scheme 2.5.[84,85] In the first steps ethylene glycol and diethylene triamine are tosylated under standard conditions. Cyclization of **2** with **1** is achieved in a two phase reaction with a catalytic amount of tetrabutylammonium hydroxide. The resulting 1,4,7-tritosyl-1,4,7-triazacyclonone **3** was detosylated twice in 33 % HBr/AcOH to yield **4**. Subsequent methylation of the monotosylated-triazacyclononane via the Eschweiler – Clarke reaction gave rise to compound **5**. Finally **5** was detosylated to obtain 1,4-dimethyl-1,4,7-triazacyclononane **6** ($M_2$-TACN), as a pale yellow liquid.

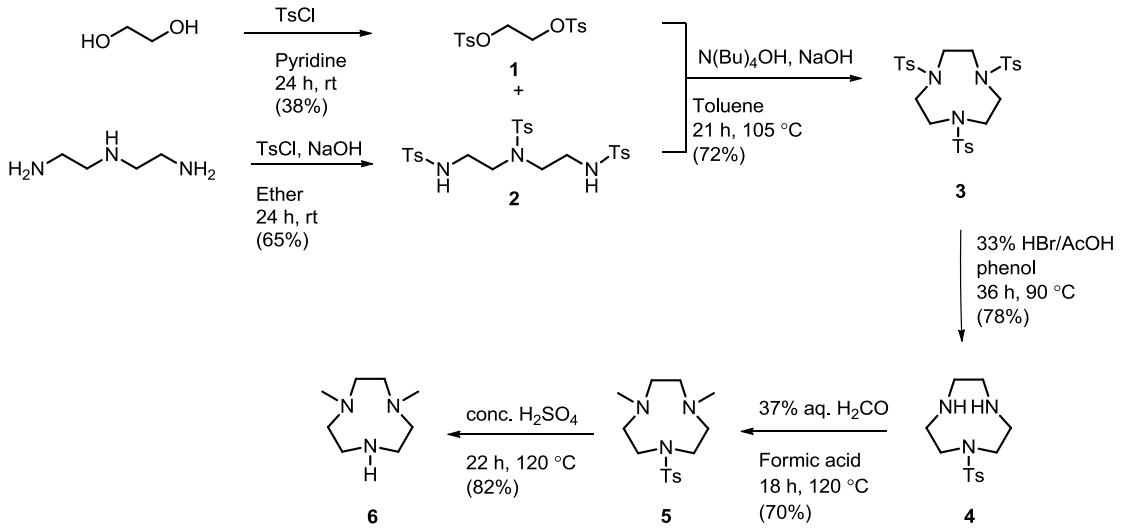


**Scheme 2.5 Synthetic route towards a TACN derivative, $M_2$-TACN that can be further functionalized.**

The $M_2$-TACN was successfully synthesized in reasonable yields, allowing further functionalization on the secondary amine to be investigated. Successful substitution of a benzyl moiety on the $M_2$-TACN ligand has lead us to explore substitution with alcohol bromides (Scheme 2.6). Unfortunately, this did not succeed; in the $^1$H NMR spectrum showed the formation of ether-like products. The formation of these adducts arose most likely due to the nucleophilic addition of alcohol with other alcohol bromides. In order to prevent this, the alcohol bromide was successfully protected with a 2-tetrahydropyrany (THP) group, to further react with $M_2$-TACN. The GC-MS trace of the reaction between the protected bromo alcohol and the $M_2$-TACN indicated the formation of the desired product.(Scheme 2.6) However, multiple impurities were observed in the GC-MS spectrum and by TLC analysis. Purification at this stage was problematic and therefore other synthetic routes towards the incorporation of pendant arm with a functional end group were explored.

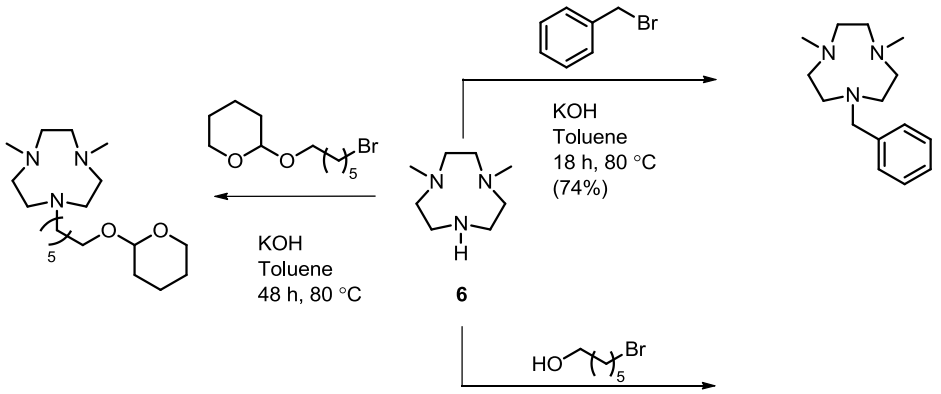


**Scheme 2.6 Substitution reactions performed on $M_2$-TACN.**

## 2.4 Results and discussion : synthesis of pendant arm incorporated TMTACN derivatives

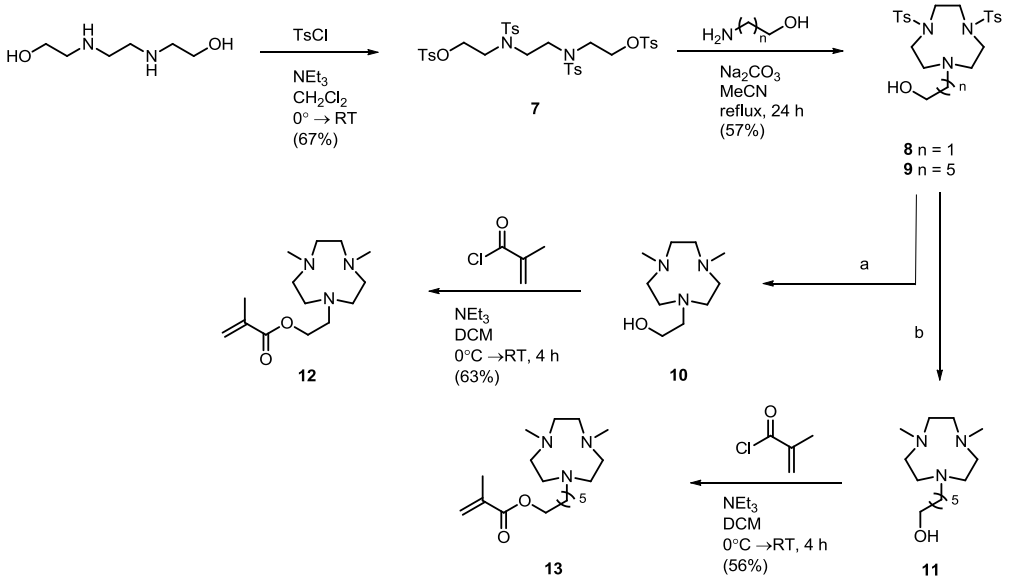


a: i) conc. $H_2SO_4$ ,115 °C, 31h ii) 37% formaldeyde/ 98% formic acid, reflux, 17 h (65%).
b: i) sodium naphtalenide, THF, -78° → RT, 18 h ii) 37% formaldeyde/ 98% formic acid, reflux, 17 h (20%).

**Scheme 2.7 Synthetic route towards a TACN derivative with a polymerizable endgroup.**

The synthetic route towards the desired TACN derivatives with a polymerizable endgroup (**12** and **13**) is depicted in Scheme 2.7. Compound **7** was obtained upon tosylation of the commercially available *N, N'*-bis(2-hydroxyethyl)ethylenediamine under standard conditions. This was reacted with 2-aminoethanol or 6-aminohexanol to obtain a ditosylated TACN derivative with a C2 - (**8**) and a C6 (**9**) spacer, respectively.[86] Compound **8** was deprotected by treatment with concentrated sulfuric acid at elevated temperatures, and the methylation reaction was performed subsequently without isolation of the unprotected products to obtain **10** in a reasonable yield.[87] Compound **9** was deprotected under the same conditions as for the deprotection of **8**, but subsequent methylation of the deprotected TACN derivative showed formation of, surprisingly, TMTACN and no indication for the formation of **11**. The detosylation reaction was therefore followed by LC-MS over time; a sample was prepared by diluting one drop of the reaction mixture in water and analyzed by LC-MS. These measurements showed cleavage of the hetero hydroxyl spacer prior to deprotection of the *N*-tosyl groups. In order to synthesize **11**, another strategy was utilized, the sulfonamide bond was cleaved under reductive conditions instead of strong acidic conditions. Compound **9** was deprotected with sodium naphtalenide and the reaction was followed by TLC until full conversion was obtained. Due to the high solubility of the deprotected amine in aqueous solutions, work up was difficult and therefore the subsequent methylation to obtain the methylated TACN **11** was performed without isolation of the deprotected triazacyclononane**.** Unfortunately a low yield was obtained, which could be due to the presence of reactive naphthalene species, which were still present despite the fact that a large quantity was removed by extraction with diethyl ether. Finally, condensation of **10** and **11** with methacryloyl chloride was performed to obtain the desired polymerizable ligand **12** and **13**, respectively.

## 2.5 Conclusion

A monofunctionalizable ligand $M_2$-TACN was obtained, but its functionalization with an alcohol moiety was not obtained because the product could not be separated from the impurities. The polymerizable ligands **12** and **13** were successfully synthesized with moderate yields following a strategy that involves direct incorporation of the functional pendent arm. Further optimization is needed to improve the synthesis of **11**, which is now hampered due to the presence of reactive naphthalene species.

## 2.6 Experimental section

General:
If not stated otherwise all chemicals used were commercial products purchased from either Acros, Sigma-Aldrich,Merck or Biosolve and used without further purification. Drop wise addition means a drop-rate ~ 1/sec. TLC analysis was performed or detection with UV – light, and/or staining added of ninhydrin or $KMnO_4$ was used. $^1$H- $^{13}$C- and 2D-NMR spectra were recorded at RT using a 400 Varian Mercury NMR spectrometer with TMS as an internal standard. IR spectra were recorded using a Perking ElmerSpectrum One FT-IR spectrometer. Interpretation of $^1$H- and $^{13}$C-, 2D-NMR spectra was done using MestReNova v6.0.2-5475, Copyright © 2009, Mestrelab Research S.L.

Synthesis of 1,2-Di(*p*-toluenesulfonyloxy)ethane (**1**)

Solid portions of TsCl (15.25 g, 0.08 mol) are added to a stirred solution of ethylene glycol (2.5 g, 0.04 mol) in pyridine (40 mL) at 0 °C over a period of 30 min. The reaction mixture was allowed to stir at room temperature for one day. Crushed ice was then added and the mixture and was placed in the fridge to stand for one day. A white precipitated solid was collected by filtration and washed with cold water, ethanol and ether. The solid was re-crystallized, which upon dissolving in a minimum amount of hot acetone and addition of ether, to yield white crystals (6.64 g, 38% yield). $^1$H NMR ($CDCl_3$, 400 MHz): δ 7.73 (d, *J* = 8.2 Hz, 4H, -$SO_2$-C-C$H_2$-), 7.34 (d, *J* = 8.1 Hz, 4H, $CH_3$-C-C$H_2$-), 4.18 (s, 4H, -C$H_2$-C$H_2$-), 2.46 (s, 6H, -C$H_3$). $^{13}$C NMR ($CDCl_3$, 100 MHz): δ 145.3, 132.3, 129.9, 127.9, 66.7, 21.7.

Synthesis of *1,4,7*- Tri(*p*-tolylsulfonyl)diethylenetriamine (**2**)

To a stirred solution of diethylenetriamine (10.4 g, 0.1 mol) and NaOH (12 g, 0.3 mmol) in $H_2O$ (100 mL), a solution of TsCl (57.2 g, 0.3 mol) in ether (300 mL) was added dropwise over a period of 60 min. The resulting mixture was stirred overnight, resulting in a white precipitate. The precipitate was collected by filtration and washed with cold water, methanol and ether. White fluffy crystals were obtained by recrystallization from hot acetone/ether (36.6 g, 65% yield). $^1$H NMR (acetone-$d_6$, 400 MHz): δ 7.75 (d, *J* = 8.2 Hz, 4H, -NH-$SO_2$-C-C$H_2$-), 7.64 (d, *J* = 8.2 Hz, 2H, -($(CH_2)_2$)N-$SO_2$-C-C$H_2$-), 7.41 (m, 6H, $CH_3$-C$H_2$-), 6.55 (br s, 2H, -N*H*-),3.13 (m, 8H, -NH-C$H_2$-C$H_2$-N-), 2.43 (s, 9H, -C$H_3$). $^{13}$C

NMR(acetone-$d_6$ ,100 MHz): δ 143.7, 143.1, 137.9, 135.93,129.8, 129.6, 127.2, 126.9, 49.3, 42.2, 20.5.

Synthesis of 1,4,7-Tri(*p*-tolylsulfonyl)-1,4,7-triazacyclononane (**3**)

To a suspension of **2** (4.97 g, 8.46 mmol) in toluene (80 mL), NaOH (2M, 9.7 mL, 19.4 mmol) and aqeous tetrabutylammonium hydroxide (1.5 M, 0.58 mL, 0.87 mmol) was subsequently added. The reaction mixture was heated to 110 °C. After 30 minutes **1** (3.27 g, 8.82 mmol) was added scoopwise in portions of ~0.12 g per 10 minutes during 4 h while refluxing. After complete addition, the reaction mixture was continued to reflux for 3 h. This was cooled down and stirred at room temperature overnight. Next day, a white sold had formed. The solid was filtrated, washed with cold water, ethanol and ether to yield a white solid (6.1 g, 72% yield). $^1$H NMR ($CDCl_3$, 400 MHz): δ 7.70 (d, *J* = 8.2 Hz, 6H, -$SO_2$-C-C$H_2$-), 7.30 (d, *J* = 8.1 Hz, 6H, $CH_3$-C$H_2$-), 3.42 (s, 12H, -N-C$H_2$-), 2.44 (s, 9H, -C$H_3$). $^{13}$C NMR($CDCl_3$, 100 MHz): δ 143.9, 143.6, 129.8, 127.5, 51.9, 30.9, 21.5.

Synthesis of 7-(*p*-tolylsulfonyl)-1-4,7-triazacyclononane (**4**)

A solution of **3** (3.7 g, 6.26 mmol) and phenol (4.4 g, 46.8 mmol) in 33% HBr in AcOH (50 mL) was stirred at 90 °C for 36 h. The mixture was neutralized by the addition of aqeous $K_2CO_3$. The solvent was evaporated to yield a sand colored solid. The solid was dissolved in 1M NaOH (30 mL) and was extracted with $CHCl_3$ (3 × 30 mL). The organic layer was dried with $MgSO_4$, filtered and concentrated in *vacuo* to yield a yellow oil (1.38 g, 78% yield). $^1$H NMR ($CDCl_3$, 400 MHz): δ 7.69 (d, *J* = 8.3 Hz, 2H, -$SO_2$-C-C$H_2$-), 7.31 (d, *J* = 8.0 Hz, 2H, $CH_3$-C$H_2$-), 3.20 – 3.08 (m, 8H, -NH-C$H_2$-C$H_2$-NTs), 2.90 (s, 4H, -NH-C$H_2$-C$H_2$-NH-), 2.42 (s, 3H, -C$H_3$). $^{13}$C NMR ($CDCl_3$, 100 MHz): δ 143.2, 135.6, 129.6, 127.2, 54.0, 30.9, 49.6, 49.5, 21.5.

Synthesis of 1,4-dimethyl-7-(*p*-tolylsulfonyl)-1,4,7-triazacyclononane (**5**)

To a solution of **4** (0.91 g, 3.28 mmol) in $H_2O$ ( 0.7 mL), 37% formaldehyde (2.1 mL, 27.8 mmol) and formic acid (2.1 mL, 55.6 mmol) was added at 0 °C. The reaction mixture was refluxed over a period of 21 h. The resulting mixture was allowed to cool to rt and HCl (1M, 1.1 mL) was added, and concentrated *in vacuo*. The residue was dissolved in $H_2O$ (2.5 mL) and 2M NaOH (3 mL) was added, upon a white solid precipitated. The solid was filtered off and washed with 2M NaOH (2 × 2mL) and $H_2O$ (2 × 2mL) to yield **5** (0.72 g, 70% yield) as a white foamy solid. $^1$H NMR ($CDCl_3$, 400 MHz): δ 7.67 (d, *J* = 8.1 Hz, 2H, -$SO_2$-C-C$H_2$), 7.30 (d, *J* = 8.3 Hz, 2H, $CH_3$-C$H_2$-), 3.08 (dt, *J* = 4.3 Hz, 8H, TsN-C$H_2$-C$H_2$-N), 2.69 (s, 4H, -($CH_3$)N-C$H_2$-C$H_2$-N($CH_3$)-), 2.42 (s, 3H, -C-C$H_3$), 2.39 (s, 6H, -N-C$H_3$). $^{13}$C NMR($CDCl_3$, 100 MHz): δ 143.0, 135.9, 129.6, 127.1, 57.5, 57.0, 51.3, 21.5.

Synthesis of 1,4-dimethyl-1,4,7-triazacyclononane (**6**)

Compound **5** (1.47 g, 4.7 mmol) was dissolved in concentrated $H_2SO_4$ (6.2 mL) and stirred at 120 °C for 21 h under argon. After cooling to rt the reaction mixture was poured into 5 g of crushed ice. The pH of the water layer was made adjusted to pH = 13 by the addition of 10M NaOH (17.5 mL). The product was extracted from the water layer with $CHCl_3$ (3 × 20 mL). The organic layer was dried with $MgSO_4$, filtered and concentrated *in vacuo* to yield **6** (0.61 g, yield 82%) as a yellow oil. $^1$H NMR ($CDCl_3$, 400 MHz): δ 2.73-2.55(m, 8H, -NH-C*H*$_2$-C*H*$_2$-N($CH_3$)-), 2.53 (s, 4H, -($CH_3$)N-C*H*$_2$-C*H*$_2$-N($CH_3$)-), 2.41 (s, 6H, -C*H*$_3$). $^{13}$C NMR($CDCl_3$, 100 MHz): δ 54.0, 52.7, 45.6, 45.1.

Synthesis of tetratosyl-*N, N'*- bis (2-hydroxyethyl) ethylenediamine (**7**)

To a solution of *N, N'*- bis (2-hydroxyethyl) ethylenediamine (7.54 g, 0.051 mol) and $NEt_3$ (35.5 mL, 0.25 mol) in DCM (40 mL) a solution of TsCl (38.9 g, 0.20 mmol) in DCM (90 mL) was added dropwise. After the addition was completed, the reaction mixture was allowed to stir at rt overnight. The mixture was washed with $H_2O$ (300 mL), 1M HCl (2 x 100 mL), sat. $NaHCO_3$ (2 x 100 mL) and brine (2 x 100 mL), The organic layer was dried with $Na_2SO_4$, filtered and concentrated *in vacuo* to yield a dark yellow oil. The oil was dissolved in hot EtOH, upon which **7** immediately precipitated (27.4 g, 70% yield) as white solid. $^1$H NMR ($CDCl_3$, 400 MHz): δ 7.77 (d, *J* = 8.3 Hz, 4H, -O-$SO_2$-C-C*H*$_2$-), 7.71 (d, *J* = 8.3 Hz, 4H, -N-$SO_2$-C-C*H*$_2$-), 7.34 (d, *J* = 8.3 Hz, 8H, $CH_3$-C*H*$_2$-), 4.14 (t, *J* = 5.4 Hz, 4H, -O-C*H*$_2$-$CH_2$-N-), 3.36 (t, *J* = 5.4 Hz, 4H, -O-$CH_2$-C*H*$_2$-N-), 3.30(s, 4H, -N-C*H*$_2$-C*H*$_2$-N-), 2.44 (s, 12H, -C*H*$_3$)

Synthesis of 2-(4,7-ditosyl-1,4,7-triazonan-1-yl)ethanol (**8**)

To a suspension of **8** (7.65 g, 10 mmol) and $Na_2CO_3$ (10.6 g, 100 mmol) in MeCN (100 mL), ethanolamine (0.6 mL, 10 mmol) was added. The suspension was allowed to reflux for 24 h. After cooling to rt the solid was filtered off and concentrated *in vacuo*. The residue was purified by column chromatography ($SiO_2$, EtOAc) to afford **8** (2.7 g, 57% yield) as a colorless oil. $^1$H NMR ($CDCl_3$, 400 MHz): δ 7.66 (d, *J* = 8.3 Hz, 4H, -$SO_2$-C-C*H*$_2$-), 7.32 (d, *J* = 8.0 Hz, 4H, $CH_3$-C*H*$_2$-), 3.61 (t, *J* = 4.9 Hz, 2H, -C*H*$_2$-OH), 3.42 (s, 4H, TsN-C*H*$_2$-C*H*$_2$-NTs), 3.25 (s, 4H, TsN-C*H*$_2$-$CH_2$-N(($CH_2$)$_2$)-), 3.01 (t, *J* = 4.8 Hz, 4H, TsN-$CH_2$-C*H*$_2$-N(($CH_2$)$_2$)-), 2.79 (t, *J* = 5.0 Hz, 2H, -N-C*H*$_2$-$CH_2$-OH), 2.43 (s, 6H, -C*H*$_3$). $^{13}$C NMR($CDCl_3$, 100 MHz): δ 143.7, 135.1, 129.8, 127.1, 60.3, 59.3, 55.1, 53.2, 52.8, 21.5.

Synthesis of 6-(4,7-ditosyl-1,4,7-triazonan-1-yl)hexanol (**9**)

Following a similar procedure as for **8**, using aminohexanol instead of ethanolamine, **9** was obtained as a white solid in 74% yield. $^{1}$H NMR ($CDCl_3$, 400 MHz): δ 7.66 (d, *J* = 8.3 Hz, 4H, -$SO_2$-C-C*H*$_2$-), 7.31 (d, *J* = 8.0 Hz, 4H, $CH_3$-C*H*$_2$-), 3.63 (m, 2H, -C*H*$_2$-OH), 3.50 (s, 4H, TsN-C*H*$_2$-C*H*$_2$-NTs), 3.17 (s , 4H, TsN-C*H*$_2$-$CH_2$-N(($CH_2$)$_2$)-), 2.85 (t, *J* = 4.8 Hz, 4H, TsN-$CH_2$-C*H*$_2$-N(($CH_2$)$_2$)- ), 2.54 (t, *J* = 7.1 Hz, 2H, -(($CH_2$)$_2$)N-C*H*$_2$-), 2.43 (s, 6H, -C*H*$_3$) 1.59-1.53 (m, 2H, -C*H*$_2$-$CH_2$-OH), 1.49-1.40 (m, 2H, -N-$CH_2$-C*H*$_2$-), 1.39-1.31 (m, 4H, -(C*H*$_2$)$_2$-($CH_2$)$_2$-OH) $^{13}$C NMR($CDCl_3$, 100 MHz): δ 143.5, 135.2, 129.8, 127.2, 62.8, 57.3, 55.8, 52.5, 51.4, 32.6, 27.7, 27.1, 25.6, 21.5.

Synthesis of 2-(4,7- dimethyl-1,4,7-triazonan-1-yl)ethanol (**10**)

A solution of **8** (5.37 g, 11.9 mmol) in conc. $H_2SO_4$ (55 mL) was heated at 115 °C over a period of 21 h. The reaction mixture was allowed to cool to 0 °C, and was neutralized to pH = 7-8 upon slow addition of 10 M NaOH. To the neutralized reaction mixture 37% formaldehyde (10.6 mL, 143 mmol) and formic acid (9 mL, 238 mmol) was added subsequently. The solution was allowed to reflux for 19 h, cooled to rt, and the pH of the water was adjusted to pH = 13 with the addition of 5M NaOH. The product was extracted from the water layer with $CHCl_3$ (3 × 300 mL). The organic layer was dried with $MgSO_4$, filtered and concentrated *in vacuo* to yield **10** as a yellow oil (1.66 g, 69%). $^{1}$H NMR ($CDCl_3$, 400 MHz): δ 3.58 (t, *J* = 5.2 Hz, 2H, -C*H*$_2$-OH), 2.77 (t, *J* = 5.3 Hz, 2H, -N-C*H*$_2$-$CH_2$-OH ), 2.74-2.66 (m, 12H, -N-C*H*$_2$-C*H*$_2$-N-), 2.38 (s, 6H, -C*H*$_3$). $^{13}$C NMR($CDCl_3$, 100 MHz): δ 60.6, 58.9, 57.9, 57.5, 55.5, 46.1.

Synthesis of 6-(4,7- dimethyl-1,4,7-triazonan-1-yl)hexanol (**11**)

To a solution of **9** (0.93 g, 1.72 mmol) in dry THF (5 mL) a solution of sodium naphtalenide (prepared *in situ* by dissolving naphthalene (1.94 g, 15.2 mmol) and sodium (0.3 g, 13 mmol)) in dry THF (20 mL) was added dropwise at -78 °C. The reaction mixture was allowed to stir overnight at rt, and quenched by addition of $H_2O$ (0.6 mL), subsequently neutralized by the addition of 2M HCl (7.5 mL) and THF was evaporated. The resulting suspension was extracted with ether (5 × 20 mL) to remove any naphthalene byproduct and the water layer was neutralized to pH = 8 by addition of 2M NaOH.

To the water layer 37% formaldehyde (1.53 mL, 20.58 mmol) and formic acid (1.29 mL, 34.3 mmol) were added, and the reaction mixture was refluxed over a period of 22 h. The reaction mixture was allowed to cool to rt, and the pH of the water layer was adjusted to pH = 13 by addition of 2M NaOH. The product was extracted from the water layer with $CHCl_3$ (4 × 20 mL). The organic layer was dried with $MgSO_4$, filtered and concentrated *in vacuo*. The residue was purified by column chromatography ($Al_2O_3$, 1% MeOH in $CHCl_3$) to afford **11** as a yellow oil (76. mg, 20%). $^{1}$H NMR ($CDCl_3$, 400 MHz): δ 3.62 (t, *J* = 6.6 Hz, 2H, -C*H*$_2$-OH), 2.77 (s, 4H, -N-C*H*$_2$-$CH_2$-N($CH_3$)-), 2.69 (s, 8H, -C*H*$_2$-N($CH_3$)- ), 2.47 (t, *J* = 7.2 Hz, 2H, -(($CH_2$)$_2$)N-C*H*$_2$-), 2.36 (s, 6H, -C*H*$_3$), 1.60-1.53 (m, 2H, -C*H*$_2$-$CH_2$-OH), 1.49-1.41 (m, 2H, -N-$CH_2$-C*H*$_2$-), 1.39-1.27 (m, 4H, -(C*H*$_2$)$_2$-($CH_2$)$_2$-OH). $^{13}$C NMR($CDCl_3$, 100 MHz): δ 62.6, 59.2, 57.4, 56.7, 56.2, 46.6, 32.8, 27.9, 27.2, 25.6.

Synthesis of 2-(4,7- dimethyl-1,4,7-triazonan-1-yl)ethylmethacrylate (**12**)

To a stirring solution of **10** (100 mg, 0.5 mmol) and $NEt_3$ (0.12 mL, 0.86 mmol) in DCM (10 mL), methacryloyl chloride (0.073 mL, 0.74 mmol) was added dropwise at 0 °C. After addition was completed, the reaction mixture was allowed to warm to room temperature and stirred for 4 h. DCM (20 mL) was added, and the product was extracted from the DCM layer with $H_2O$ (20 mL). The water layer was extracted with $CHCl_3$ (2 × 20 mL). The pH of the water layer was adjusted to pH = 13 by the addition of 2M NaOH and extracted with $CHCl_3$ (2 × 20 mL). The combined organic layer was dried with $MgSO_4$ and concentrated *in vacuo*. The residue was purified with column chromatography ($Al_2O_3$, 1% MeOH in $CHCl_3$) to yield **12** as a pale yellow oil (85 mg, 63% yield). $^1$H NMR ($CDCl_3$, 400 MHz): δ 6.12 (m, 1H,-C=C(H)*H*), 5.56 (m, 1H, -C=C(*H)*H), 4.22 (t, *J* = 6.0 Hz, 2H, -C*H*$_2$-O(C=O)), 2.85 (t, *J* = 6.0 Hz, 2H, -N-C*H*$_2$-CH$_2$-O-), 2.79-2.66 (m, 12H, -N-C*H*$_2$-C*H*$_2$-N- ), 2.36 (s, 6H, -N-C*H*$_3$), 1.95 (m, 3H, -C-C*H*$_3$) (Appendix A). $^{13}$C NMR($CDCl_3$, 100 MHz): δ 167.2, 136.2, 125.3, 63.0, 57.2, 57.0, 56.6, 56.5, 46.5, 18.3. FT-IR(v, cm$^{-1}$): 2926 s, 2838 s, 2785 s, 1718 s, 1877 m, 1638 w, 1520 s, 1495 s, 1453 s, 1367 m, 1318 m, 1295 s, 1157 s, 1111 s, 1033 s, 1003 s, 941 w, 815 w. (Appendix C) Maldi-TOF MS : Calculated [M-$ClO_4$]$^+$ = 269.21 Da, observed [M+H]$^+$ = 270.28 Da (Appendix B)

Synthesis of 2-(4,7- dimethyl-1,4,7-triazonan-1-yl)hexylmethacrylate (**13**)

Following the same procedure as for **12**, compound **13** was obtained as yellow oil in 56% yield. $^1$H NMR ($CDCl_3$, 400 MHz): δ 6.12 (m, 1H, -C=C(H)*H* ), 5.52 (m, 1H, -C=C(*H)*H ), 4.12 (t, *J* = 6.7 Hz, 2H, -C*H*$_2$-OH), 2.72 (s, 4H, -N-C*H*$_2$-CH$_2$-N(CH$_3$)-), 2.65 (s, 8H, -C*H*$_2$-N(CH$_3$)-), 2.44 (t, *J* = 7.2 Hz, 2H, -((CH$_2$)$_2$)N-C*H*$_2$-), 2.34 (s, 6H, -N-C*H*$_3$), 1.92 (m, 3H, C-C*H*$_3$), 1.69-1.62 (m, 2H, -C*H*$_2$-CH$_2$-O(C=O)), 1.47-1.39 (m, 2H, -N-CH$_2$-C*H*$_2$-), 1.37-1.29 (m, 4H, -(C*H*$_2$)$_2$-(CH$_2$)$_2$-O(C=O)). (Appendix A)

# Chapter 3 Synthesis and characterization of TMTACN based copper(II) complexes

## 3.1 Introduction to (TM)TACN coordination chemistry

The tridentate macrocyclic triazacyclononane ligand is known to form stable coordination complexes with various metals, i.e. with the heavier main group elements (Ga, In, Tl and Pb) and almost all transition metals.[88] The stable coordination is due to donation of the sigma orbital of the ligand to the d-orbitals of the metal. Macrocycles of larger ring sizes form less stable complexes, which is ascribed to the poor overlap between the donor-acceptor orbitals.[89] TACN ligands usually coordinate with metals in a 2:1 fashion to obtain pseudo-octahedral complexes (Figure 3.1).[90] In contrast, TMTACN ligands only form 1:1 ligand to metal complexes, due to the steric hindrance of the methyl groups that prevents coordination of the two ligands in an octahedral arrangement.[77]

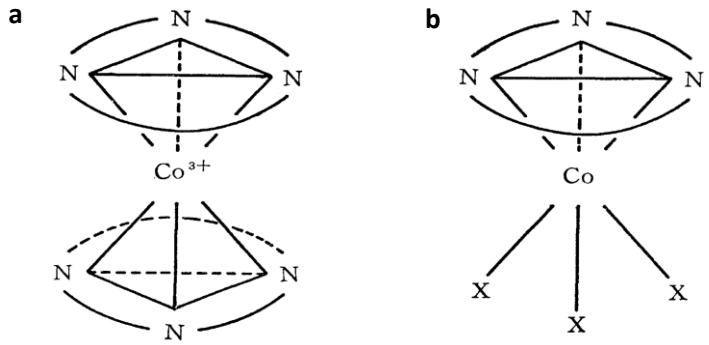


**Figure 3.1 Schematic overview of TACN – metal coordination. (a) Cobalt(III) is sandwiched in between two facially coordinating TACN ligands (b) Mono-TACN - cobalt(III) complex facilitates the coordination of unidentate (X) ligands.**

The TMTACN ligand is facially capping the metal that facilitates coordination of unidentate ligands (X) on the other metal end (Figure 3.1). The formation of $LMX_3$ - type of ligands, in which X can be readily substituted, can be used as an effective precursor for dinuclear [LM(bridge)$_n$LM] complexes.[88]

### 3.1.1 TMTACN – and TACN derivatized copper(II) based complexes

TMTACN based copper complexes can adopt different coordination geometries depending on the substitution on the amine and coordination of unidentate or chelating ligands on the remaining coordination site (Figure 3.2). Crystal structures on TMTACN-Cu(II) complexes with two water molecules coordinated [**C1**] showed that this complex adopts a distorted octahedral geometry.[91] When this mononuclear complex is treated with one equivalent of sodium oxalate, dimeric oxalate bridged copper complexes [**C2**] are formed.[91] Binding of oxalate introduces geometrical constraints on the metal that lead to a trigonal bypyramidal coordination. It has also been shown that the two

apical nitrogen atoms orient in a trans configuration. This could also be seen when a benzyl functionalized TMTACN derivative was complexed to a copper that was bridged by an oxalate anion [**C3**].[91] The nitrogen pendant arm occupies the apical positions; this complex adopts a similar geometry as compared to complex [**C2]**.

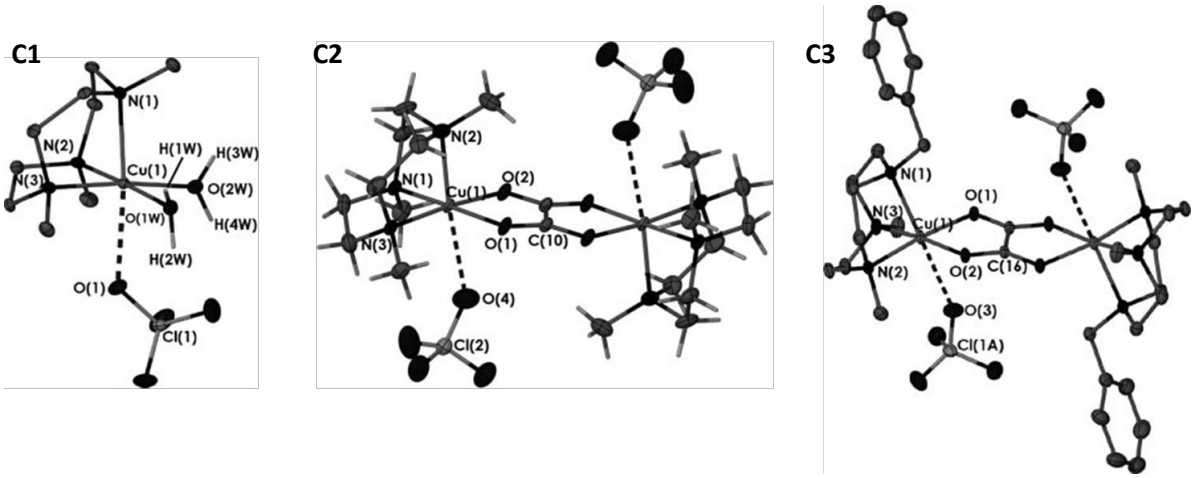


**Figure 3.2 Crystal structures of TMTACN based copper complexes.**

## 3.2 Results and discussion: Synthesis of TMTACN based copper complexes

### 3.2.1 Preparation of TMTACN based complexes

In order to investigate the activity of a model complex prior to the mechanical activation of the mechanocatalyst, various TMTACN-copper complexes were synthesized. The mononuclear diaqua copper complex is known to act as an active species in the hydrolysis reaction, whereas both the di-μ- hydroxo and oxalate bridged copper complexes are expected to be inactive in the hydrolysis reaction.

The TMTACN – copper complexes were successfully synthesized using adapted procedures described in literature (Scheme 3.1).[66,91,92] The mononuclear TMTACN (L1) based copper complex, which has two coordinating water ligands, **[L1Cu($H_2O$)$_2$]** was synthesized by treating copper perchlorate hexahydrate ($Cu(ClO_4)_2 \cdot 6H_2O$) with the TMTACN ligand in a 1:1 stoichiometry. Subsequently, the slightly acidic mixture was adjusted to near neutral pH and concentrated slowly in order to form the mononuclear complex. The oxalate bridged complex **[L1Cu-μ-Ox]** was obtained upon refluxing **[L1Cu($H_2O$)$_2$]** with sodium oxalate in water. In contrast to what is reported in literature, the complex did not dissolve in a hot MeOH/ EtOH solution, and therefore, the powder could not be recrystallized. The di-μ-hydroxo bridged TMTACN-Cu(II) complex **[L1Cu-μ-OH]** was prepared by reaction of copper perchlorate hexahydrate with a slight excess of TMTACN ligand in methanol. During the reaction **[L1Cu-μ-OH]** precipitated out as a blue powder.

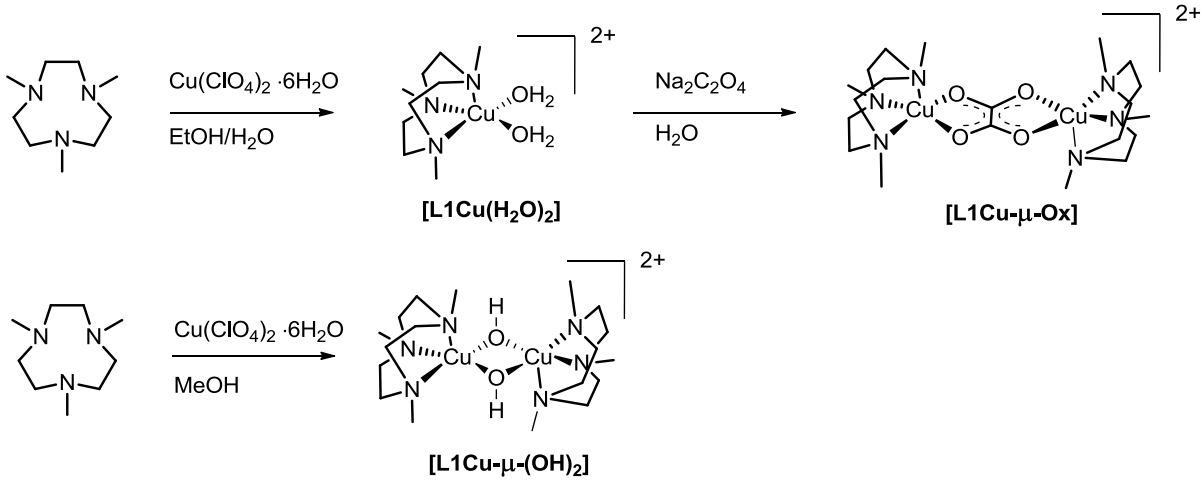


**Scheme 3.1 Synthetic scheme of three TMTACN based copper(II) complexes.**

Our first attempt to synthesize copper complexes with the polymerizable ligand were not successful. Treating the ligand with $Cu(ClO_4)_2$ in an $MeOH/H_2O$ solution and addition of aqeous sodium oxalate solution, led to the hydrolysis of the methacrylate ester. Based on a literature procedure, in which solvolysis of a TACN ligand functionalized with nitrile groups is prevented by changing the order of adding reagents to the reaction mixture.[93] Firstly, both oxalate and TMTACN derived ligands are mixed in solution, and the copper is added afterwards. Due to larger reactivity of the TMTACN derived ligands and oxalate anions with copper, the solvent molecules are prevented to coordinate to the metal ion. In this way, nucleophilic attack of solvent molecules on the methacrylate ester of the ligand can be avoided. (Scheme 3.2)

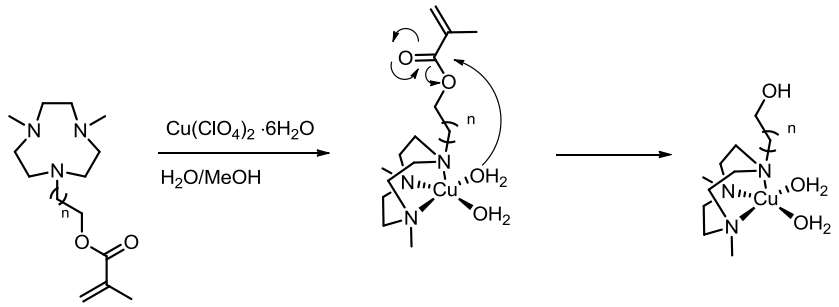


**Scheme 3. 2 Hydrolysis of methacrylate ester by the coordinated water molecules on the copper(II) center**

The synthesis of copper complexes with compounds **12** and **13** (see Chapter 2) was achieved by treating the ligand with sodium oxalate followed by addition of copper perchlorate hexahydrate. (Scheme 3.2) The resulting mixture was stirred over a period of 1.5 h before evaporating the solvent. The dinuclear oxalate bridged **[L2Cu-μ-Ox]** and **[L3Cu-μ-Ox]** were obtained upon recrystallization from acetonitrile/ether.

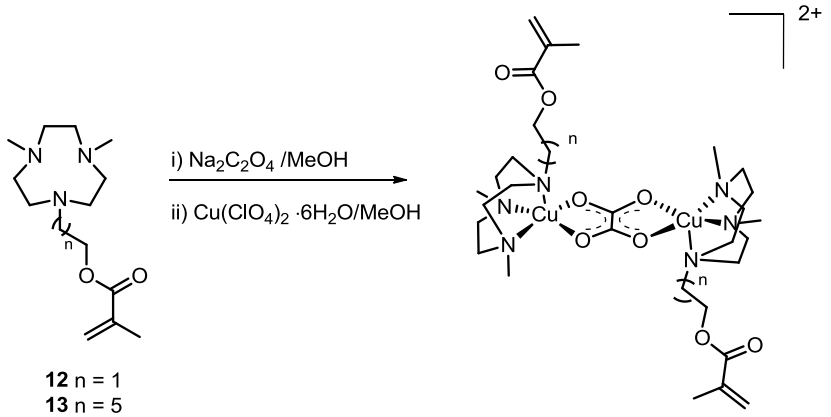


**Scheme 3.3 Synthesis of polymerizable TMTACN copper(II) complexes.**

### 3.2.2 Characterization of the TMTACN copper(II) complexes

A frequent used characterization technique of organic molecules is nuclear magnetic resonance (NMR) spectroscopy. For copper complexes that consist of a paramagnetic $Cu^{2+}$ center, i.e. the metal contains one or more unpaired electrons, NMR spectroscopy is a less obvious choice of characterization. Due to the presence of unpaired electrons, small local magnetic fields are generated. This will influence the field experienced by an H nuclei during a $^1H$ NMR measurement, and often results in large difference in chemical shift and broadening of the signals, which makes the characterization of the complex more difficult.

Coordination complexes of copper(II) are therefore often characterized with spectroscopic techniques such as ultraviolet-visible-near infrared (UV-Vis-NIR) spectroscopy and infrared (IR) spectroscopy. Both UV-Vis-NIR and IR spectroscopy methods measures the absorbance of electromagnetic irradiation from the coordination complex, that can originate from energy transitions of orbitals or transitions from vibrational movements, respectively. Matrix-assisted laser desorption/ionization – time of flight (MALDI-TOF) mass spectrometry can be used to identify mass to charge ratios of complexes and due to the soft ionization method, decomposition of the complex may be prevented.

#### 3.2.2.1 Introduction to the various characterization methods used in this study

**UV-Vis-NIR spectroscopy**

Most of the d-block coordination complexes absorb light; their presence is therefore often rich in color. The transitions that are observed may originate from the transition between the metal centered orbitals (d-d transition) or from transitions between the metal and ligand centered molecular orbitals (charge transfer bands).[94]

In a UV-Vis-NIR measurement, a region of 100-1400 nm will be irradiated on a sample.[95] The absorbance of light results in transitions between energy levels of the coordination complex. In the spectrometer the detector records the transmission (T) of light. The transmission of light is correlated to the absorbance (A), as

$$A = - \log (T) \qquad (3.1)$$

The absorbance is dependent on the concentration of the sample (c), the pathway of light that travels through the sample (l) and the molar absorptivity (ε), which gives a measure on how much light is absorbed at each wavelength. The factors that influence the absorbance are given by the Beer – Lambert law[95] (2):

$$A = \varepsilon \times l \times c \qquad (3.2)$$

**IR spectroscopy**

In infrared spectroscopy absorption is only observed when an electric dipole moment changes during movement of the molecule.[94] The movement of the molecule is related to the degree of vibrational freedom. For a polyatomic molecule (consisting of *n* atoms) the degree of freedom is *3n*, when the motion of a molecule is described with the Cartesian axes. Apart from vibrational motion, a molecule has translational and rotational motion. To deduce the degree of vibrational freedom, the remaining motions should be subtracted to give a degree of vibrational freedom of *3n-6* for a non-linear molecule and *3n-5* for a linear molecule. The types of vibrational modes of a non-linear $CH_2$ group are depicted in Figure 3.3.

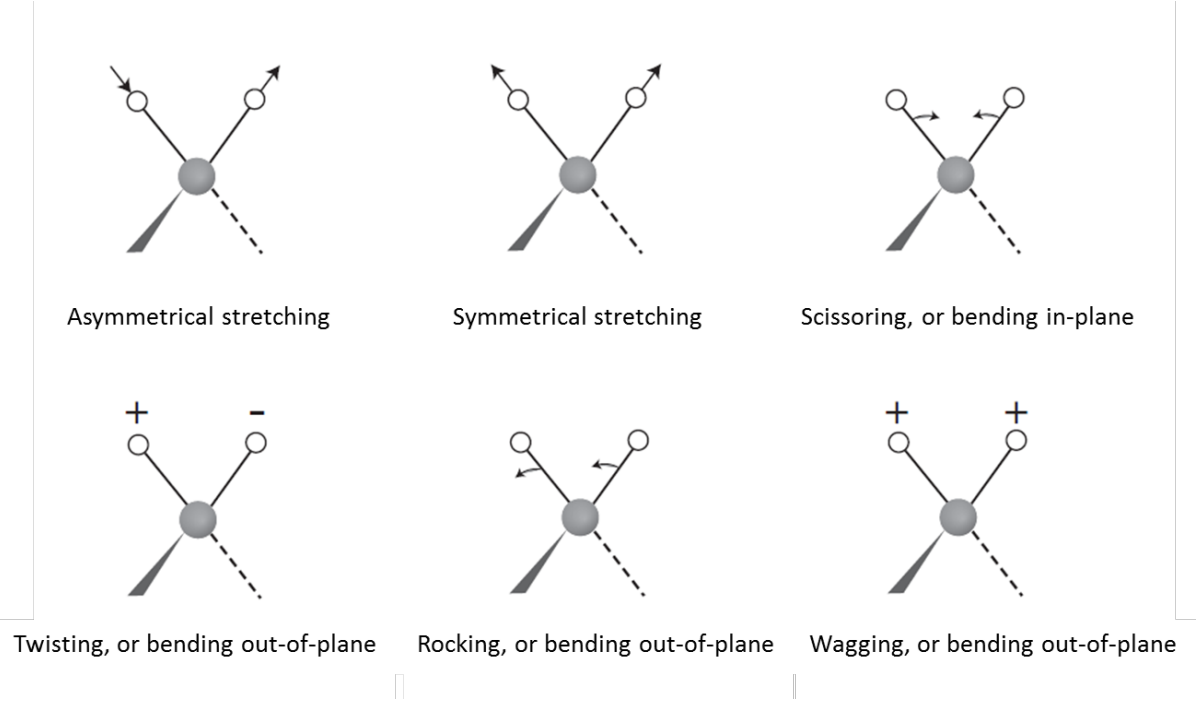


**Figure 3.3 Types of vibration modes of a methylene group.**

IR spectroscopy measures the transmission resulted by irradiation of the sample, covering the electromagnetic spectrum from 400-4000 $cm^{-1}$.[95] The transmission can be measured by an attenuated total reflectance (ATR) accessory,[96] which consist of a crystal with a high refractive index. Irradiation of an infrared beam at a certain angle onto the crystal gives rise to internal reflectance that creates an evanescent wave that is extended throughout the crystal. A sample that is in contact with the crystal adsorbs energy, resulting in the attenuation or alteration of the evanescent wave. The altered wave is detected by the exiting wave at the opposite end of the crystal.

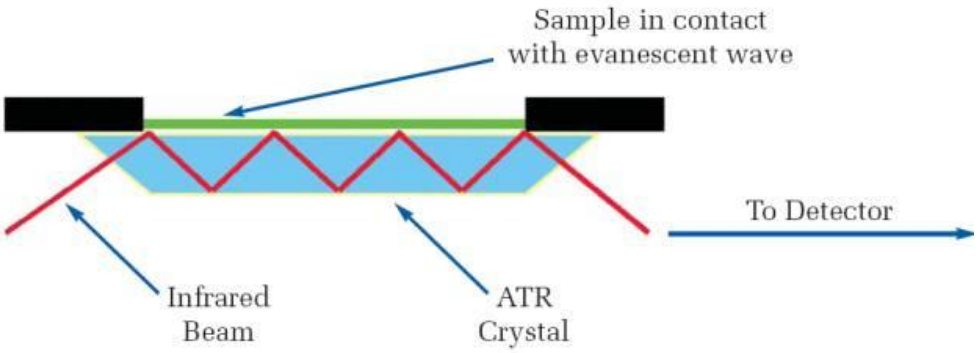


**Figure 3.4 Schematic overview on the working principle of an ATR accessory; irradiation of an IR beam on the ATR crystal is reflected and leads to formation of evanescent wave. Adsorption of energy by the sample leads to attenuation of the evanescent wave that can be detected.**

### MALDI-TOF mass spectrometry

For the MALDI-TOF mass spectrometry technique,[97] analyte is embedded in a matrix that consists of a crystalline structure of small organic molecules. The matrix with embedded analyte is irradiated with a nanosecond laser beam that causes structural decomposition of the co-crystals. From the decomposition a particle cloud of ions is generated. The ions are accelerated through an electric field and reach the detector upon ion-drift through a field-free path. The mass detection, given by the mass to charge ratio [m/z], is correlated to the time of flight of the ion masses. (Figure 3.4)

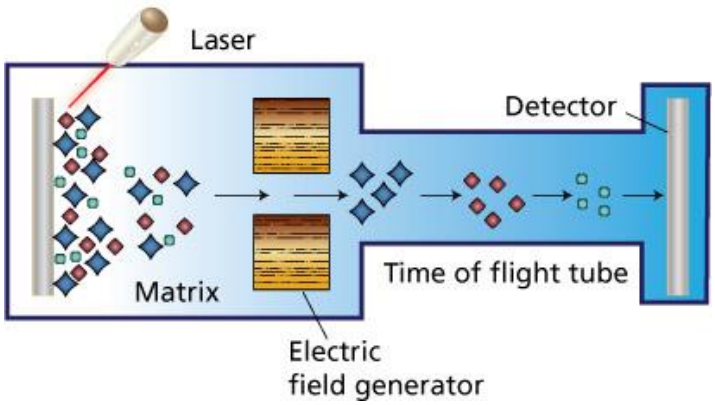


**Figure 3.5 Schematic overview of MALDI-TOF spectroscopy; upon irradiation of a laser pulse, an ion cloud is generated, this will be accelerated through an electric field and separation of components lead to differentiation of time of flight that reaches the detector.**

### 3.2.2.2 Characterization by UV-Vis-NIR spectroscopy

The UV-Vis-NIR spectrum of the studied copper complexes in acetonitrile (MeCN) showed absorption bands in good correlation with data reported in literature. The absorption maxima and the corresponding absorption coefficients are given in Table 3.1. In the UV-Vis-NIR spectrum for all the complexes bands around λ = 280 and 620 nm are visible. The first band is indicative for the copper-TMACN coordination and is due to charge transfer to the ligand or ligand π→π* transitions. The latter band indicates that the TMTACN based copper(II) complexes are in square pyramidal geometry.

**Table 3.1 Absorption maxima and the corresponding absorption coefficient (ε) of TMTACN Cu complexes discussed in this study.**

| Complex | Wavelength / nm (ε / $M^{-1}$ $cm^{-1}$) | Wavelength /nm (ε / $M^{-1}$ $cm^{-1}$) | Wavelength / nm (ε / $M^{-1}$ $cm^{-1}$) |
|---|---|---|---|
| **[L1Cu($H_2O$)$_2$]** | 641(165) | | 292(5466) |
| **[L1Cu-μ-Ox]** | 632(243) | 333(4566) | 282(12040) |
| **[L1Cu-μ-(OH)$_2$]** | 620(154) | 364(611) | 267(6058) |
| **[L2Cu-μ-Ox]** | 630(190) | 333(2520) | 282(6896) |
| **[L3Cu-μ-Ox]** | 623(1970) | 333(1186) | 282(2986) |
| **[L1Cu-μ-Ox]** (lit. ref. 91) | 632(118) | 333(4160) | 282(11100) |

For the oxalate bridged complexes transitions observed at λ = 333 nm result either from a charge transfer or ligand π→π* transitions (Figure 3.6). In literature an absorption at λ = 1100 nm was reported, but this band was not observed for **[L1Cu-μ-Ox]**. This may be due to the low absorption coefficient of 68 $M^{-1}$ $cm^{-1}$; making it more difficult to observe the band at λ = 1100 nm in dilute solutions.

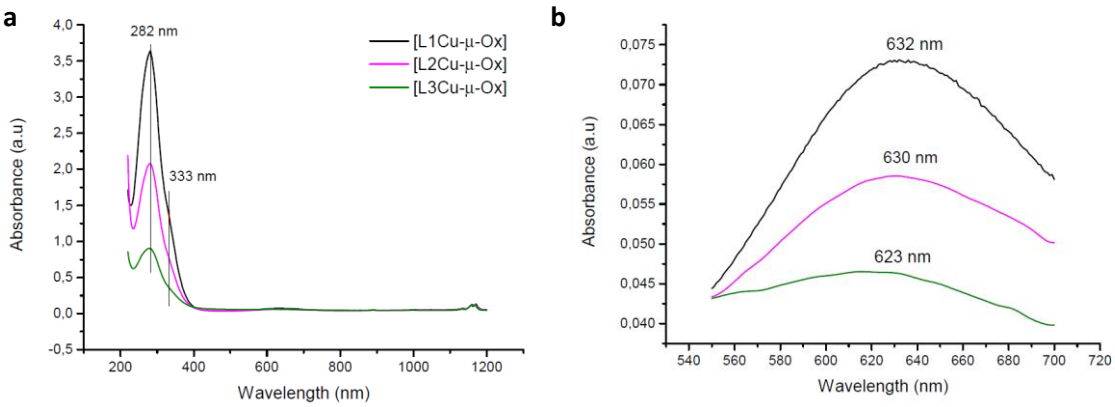


**Figure 3.6 (a) UV-Vis-NIR spectrum of oxalate bridged copper complexes ([L1Cu-μ-Ox], [L2Cu-μ-Ox], and [L3Cu-μ-Ox]) complexes show absorption maxima at λ = 282 nm and a shoulder at 333 nm. (b) The absorption maxima at around λ = 630 nm of the copper complexes.**

### 3.2.2.3 Characterization with IR spectroscopy

In Table 3.2 the characteristic vibrational bands of the TMTACN – copper(II) based complexes are summarized. Complex **[L1Cu($H_2O$)$_2$]** showed a broad band at higher frequencies, that corresponds to coordinated water. In addition, at 1624 $cm^{-1}$ the deformation mode of water is observed. In contrast to **[L1Cu($H_2O$)$_2$]**, the IR spectrum of the hydroxo-bridged **[L1Cu-μ-(OH)$_2$]** complex showed a sharp band at higher frequency due to the absence of hydrogen bonds between the two bridged alcohols. For the TMTACN oxalate bridged complex **[L1Cu-μ-Ox]**, the characteristic stretching modes of the oxalate (C=O) were observed at 1646 $cm^{-1}$ ($\nu_{asym}$) and 1466 $cm^{-1}$ ($\nu_{sym}$). These complexes showed vibrational bands that correspond to reported data in literature.[91]

**Table 3.2 Characteristic vibrational bands of synthesized complexes.**

| Complex | Wavenumber / $cm^{-1}$ * |
|---|---|
| **[L1Cu($H_2O$)$_2$]** | ν(HO) 3369 br; ν(H-O-H) 1624 w |
| **[L1Cu-μ-Ox]** | ν(C=O) 1646 s, 1466 s |
| **[L1Cu-μ-(OH)$_2$]** | ν(HO) 3618 s |
| **[L2Cu-μ-Ox]** | ν(C=O(Ox[1])) 1653 s, 1458 s; ν(C=O(MA[2])) 1715 s; ν(C-O(MA)) 1287 m, 1168 m; ν(C-H(MA)) 954 w; ν(C=C(MA)) 814 w |
| **[L3Cu-μ-Ox]** | ν(C=O(Ox[1])) 1658 s, 1464 s; ν(CO(MA[2])) 1716 s; ν(C-O(MA)) 1298 m |

* all spectra show vibrational bands at 1080 $cm^{-1}$ and 620 $cm^{-1}$ which are assigned to the perchlorate anion.

[1] Ox = oxalate anion; [2] MA = methacrylate group.

From the IR spectrum of the complex with polymerizable ligand [**L2Cu-μ-Ox]**, the characteristic C=O stretching modes of the methacrylate and oxalate moiety could be clearly distinguished. The C=C twist and the C-H out of plane bend from the methacrylate was also present in the IR spectrum. Although a clear difference between the C=O stretching from the oxalate and methacrylate group was observed for complex with the C6 analogue **[L3Cu-μ-Ox]**, the other vibrational bands (i.e., bands at 814 and 954 $cm^{-1}$) of the polymerizable group were not observed.

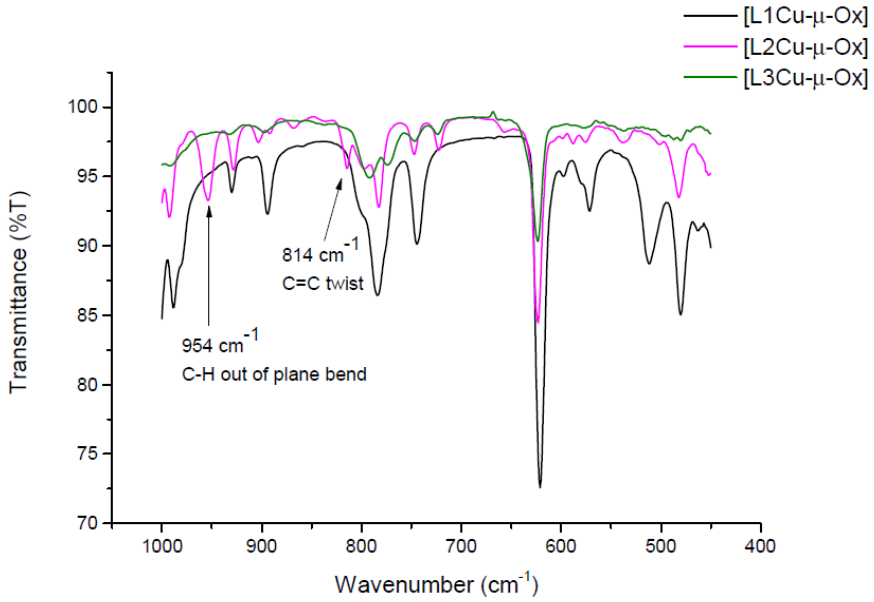


**Figure 3.7 IR spectrum of oxalate bridged copper complexes showing the vibrational bands for the [L2Cu-μ-Ox] complex in the finger print region.**

### 3.2.2.4 Characterization with MALDI-TOF mass spectrometry

The formation of the desired complexes could be confirmed by MALDI-TOF analysis, which showed a mass that corresponded with the desired copper complex with one perchlorate counterion. In case of **[L3Cu-μ-Ox]** it also showed a mass corresponding to ligand with only one copper coordinated, this may be a result from defragmentation during the ionization with the laser pulse. The defragmentation was however not observed for the **[L2Cu-μ-Ox]** complex, for reasons that are unclear.

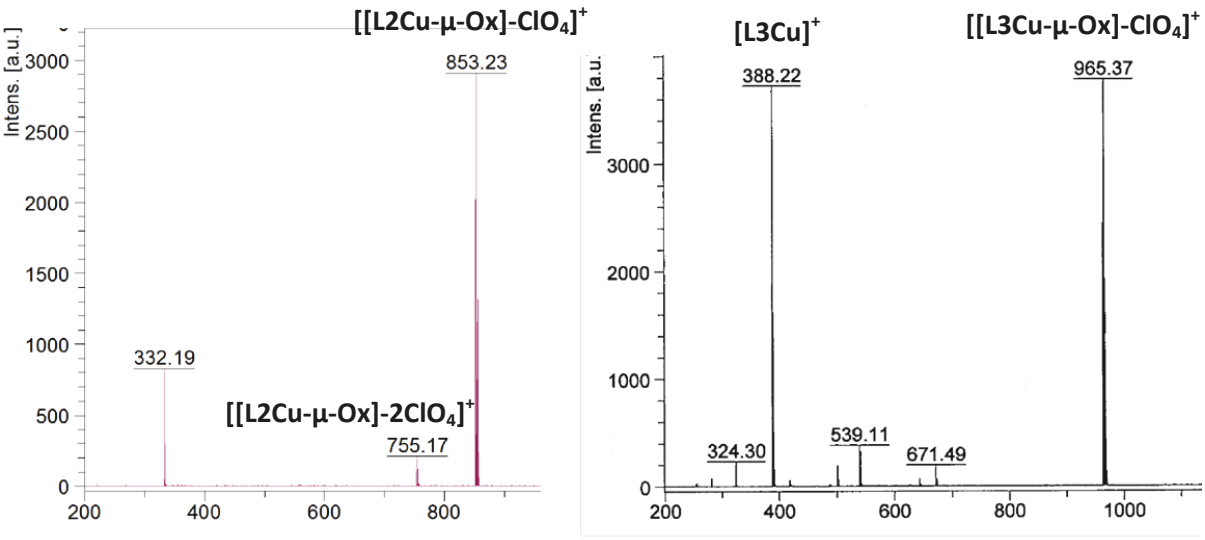


**Figure 3.8 MALDI-TOF spectra of complexes [L2Cu-μ-Ox] and [L3Cu-μ-Ox].**

## 3.3 Conclusion

The synthesis of the desired TMTACN Cu complexes was successful, as could be confirmed by UV-Vis-NIR, IR and mass spectroscopy. The UV-Vis-NIR spectrum showed a square bipyramidal coordination of the complex and coordination of the ligands. With IR spectroscopy, the vibrational bands of the methacrylate group are observed, which means that the polymerizable group is stable during the synthesis and work-up. Moreover, it could be seen that the complexes are coordinated with an oxalate anion, because these characteristic stretches could be distinguished from the stretches of the methacrylate group. Finally, MALDI-TOF MS measurements showed formation of dimeric oxalate bridged copper complexes with polymerizable side groups on the the TMTACN ligand.

## 3.5 Experimental section

General

All solvents (AR quality) and chemicals were purchased from Biosolve, Sigma- Aldrich or Acros and were used as received, unless stated otherwise. **UV-Vis-NIR spectroscopy** was performed on a Lambda 900 at rt, measurements were done with a scan rate of 750 nm/min. **IR Spectroscopy** was performed at rt on a Perkin Elmer Spectrum One FT - IR spectrometer with a universal Attenuated Total Reflectance (ATR) sampling accessory. Interpretation of the spectra was done using a Perking Elmer Spectrum version 10.03.08.0135, Copyright 2012 Perkin Elmer Inc. Background spectra were measured prior to measuring samples and automatic baseline correction was performed.
**MALDI-TOF mass spectrometry** was performed on a PerSeptive Biosystems Voyager-DE PRO

spectrometer using α-cyano-4-hydroxycinnamic acid as the matrix.

Synthesis of $[Cu(TMTACN)(H_2O)_2](ClO_4)_2$ complex **[L1Cu($H_2O$)$_2$]**

To a solution of copper perchlorate hexahydrate ($Cu(ClO_4)_2 \cdot 6H_2O$)(43 mg, 0.12 mmol) in $H_2O$ (0.2 mL), a solution of TMTACN (20 mg, 0.12 mmol, in a 1:1 EtOH/$H_2O$ mixture (0.2 mL)) was added drop-wise. The pH of this mixture was adjusted to pH = 6 by addition of one droplet of a 2M NaOH solution and slowly concentrated till dryness in a desiccator with $P_2O_5$ *in vacuo*. The residue was dissolved in EtOH (~5 mL) upon which a small amount of dark blue solid remained undissolved. The solution was isolated and diethyl ether was added until the solution became cloudy and precipitation of the product was observed. The solvent was removed upon decantation and the crystals were washed thoroughly with ether. The crystals were collected upon removal of the solvent and dried in air to yield a light blue solid (23 mg, 40% yield). FT-IR(ν, $cm^{-1}$): 3369 br m, 2883 w, 2828 w, 1624 br m, 1496 w, 1463 m, 1301 w, 1054 s, 1008 s, 935 w, 893 w, 785 w, 748 w, 621 s. UV-Vis-NIR [MeCN; $\lambda_{max}$,nm (ε, $M^{-1}$ $cm^{-1}$)]: 641(165), 292(5466).

Synthesis of $[Cu_2(TMTACN)_2(\mu\text{-}Ox)](ClO_4)_2$ **[L1Cu-μ-Ox]**

To a solution of **[L1CuH2O]** (12 mg, 0.025 mmol) in $H_2O$ (0.4 mL) was added a solution of $Na_2C_2O_4$ (3.8 mg, 0.028 mmol) in $H_2O$ (0.2 mL). This mixture was refluxed during a period of 1.5 h and then allowed to cool to rt. The resulting mixture was concentrated in a desiccator with $P_2O_5$ *in vacuo* until dryness was observed. The blue solid was washed with hot MeOH:EtOH (1:1) solution to yield dark blue crystals (9 mg, 47%). FT-IR(ν, $cm^{-1}$): 2996 w, 2967 w, 2926 w, 1648 s, 1466 s, 1353 m, 1299 m, 1071 br s, 1006 s, 784 s, 744 s, 746 s. UV-Vis-NIR [MeCN; $\lambda_{max}$,nm (ε, $M^{-1}$ $cm^{-1}$)]: 632(243), 333(4566), 282(12040).

Synthesis of $[Cu_2(TMTACN)_2(\mu\text{-}OH)](ClO_4)_2$ **[L1Cu-μ-(OH)$_2$]**

To a solution of $Cu(ClO_4)_2 \cdot 6H_2O$ (32 mg, 0.09 mmol) in $H_2O$ (1.5 mL), a solution of TMTACN (25 mg, 0.14 mmol) in MeOH (0.14 mL) was added. Upon the addition of the ligand, blue crystals precipitated immediately. This mixture allowed to stand at rt over a period of 48 h. The crystals were filtered off and washed with ethanol and ether. Dark blue crystals were obtained in low yield (8.5 mg, 13%). FT-IR(ν, $cm^{-1}$): 3618 m, 2884 m, 2828 m, 1456 m, 1302 w, 1083 s, 1008 s, 893 m, 862 m, 781 s, 745 s, 621 s. UV-Vis-NIR [MeCN; $\lambda_{max}$,nm (ε, $M^{-1}$ $cm^{-1}$)]: 620(154), 364(611), 267(6058).

Synthesis of $[Cu_2(\mathbf{12})_2(\mu\text{-}Ox)](ClO_4)_2$ **[L2Cu-μ-Ox]**

Compound **12** (8.6 mg, 0.03 mmol) and an aqueous $Na_2C_2O_4$ (4.7 mg, 0.03 mmol) solution (0.2 mL) were dissolved in MeOH (1.4 mL). To this suspension a solution of $Cu(ClO_4)_2 \cdot 6H_2O$ (12.1 mg, mmol) in MeOH (1.6 mL) was added drop-wise. The resulting mixture was stirred at rt over a period of 2.5 h. During the reaction $H_2O$ (1 mL) was added to aid the solubility of the oxalate in solution, upon which the mixture became a cloudy mixture. This solution was evaporated to dryness upon placing the solution in a desiccator with $P_2O_5$ *in vacuo*. The resulting blue solid was washed with ether and dried

in air. The solid was recrystallized upon dissolving in MeCN and addition of diethyl ether till cloudiness of the mixture and eventually precipitation of the pale blue solid (4.8 mg, 16%) was observed. FT-IR(ν, $cm^{-1}$): 2925 w, 2855 w, 1715 s, 1653 s, 1458 br m, 1298 m, 1168 m, 1085 s, 954 w, 814 w, 783 w, 623 s. (Appendix C)
UV-Vis-NIR [MeCN; $\lambda_{max}$,nm (ε, $M^{-1}$ $cm^{-1}$)]: 623(190), 333(2520), 282(6896).
Maldi-TOF MS : Calculated $[M\text{-}ClO_4]^+$ = 853.22 Da, observed $[M\text{-}ClO_4]^+$ = 853.23 Da.(Appendix B)

Synthesis of $[Cu_2(\mathbf{13})_2(\mu\text{-}Ox)](ClO_4)_2$ complex **[L3Cu-μ-Ox]**

Following a similar procedure as for **[L3Cu-μ-Ox]**, using compound **13** instead of **12**, complex **[L3Cu-μ-Ox]** was obtained in 44% yield (21.2 mg). FT-IR(ν, $cm^{-1}$): 2925 s, 2855 s, 1716 s, 1658 s, 1464 br m, 1298 w, 1096 s, 792 w, 623 s. (Appendix C) UV-Vis-NIR [MeCN; $\lambda_{max}$,nm (ε, $M^{-1}$ $cm^{-1}$)]: 623(1970), 333(1186), 282(2986). Maldi-TOF MS : Calculated $[M\text{-}ClO_4]^+$ = 965.35 Da, observed $[M\text{-}ClO_4]^+$ = 965.36 Da.

# Chapter 4 Hydrolysis reaction using TMTACN – copper(II) complexes

The ultimate goal of this research is to develop a mechanocatalyst that will be activated by mechanical stress. Since the synthesis of copper complexes consisting of polymerizable ligands proved to be successful, we will investigate the hydrolysis reaction using TMTACN – copper(II) complex as a model system. This allows us to evaluate the catalytic activity of TMTACN complexes discussed in this project, before we incorporate the complex into a network.

## 4.1 Introduction

In the mononuclear form the TMTACN copper complexes are active catalysts for the phosphate ester hydrolysis. The rates of these processes are extremely low, the catalyst only performs one catalytic cycle per day.[66] The low activity is believed to be due to dimerization of the mononuclear complex to the inactive binuclear copper complex, which prohibits coordination of the substrate. Moreover, bridging hydroxides are weaker nucleophiles as compared to terminal hydroxides.[66] In Scheme 4.1 a detailed pathway of the reactive species in the catalytic cycle is depicted. The pathway suggest that both copper complexed with water or hydroxy lead to active catalysis (i.e hydrolysis of bis(*p*-nitrophenylphosphate) (BNPP)). The hydroxy coordinated complex is more active due to the more nucleophilic character of hydroxide compared to water. The remaining *p*-nitrophenylphosphate (NPP) can be further hydrolyzed to yield phosphate. Therefore, two rate constants ($k_{obs1}$ and $k_{obs2}$) can be deduced when kinetic experiments are conducted.

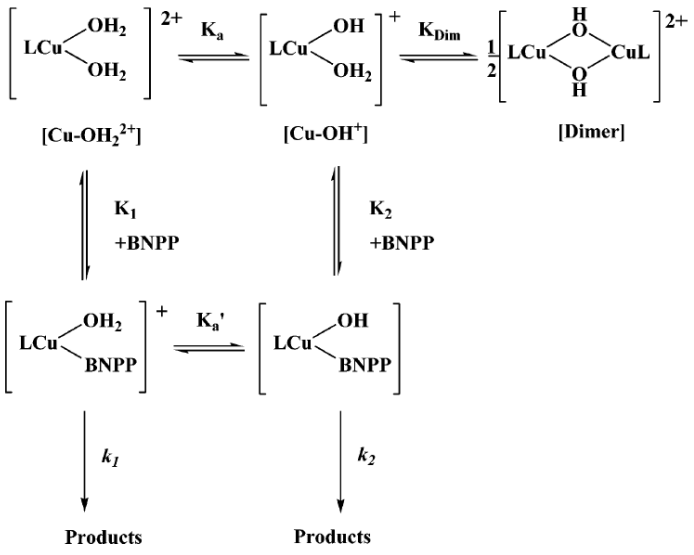


**Scheme 4.1 Reaction pathway of TMTACN-copper complexes in the hydrolysis reaction of BNPP ($K_{1,2}$ = equilibrium constant of the BNPP coordination to the complex [Cu-$OH_2^{2+}$] and [Cu-$OH^+$], respectively , $k_{1,2}$ = rate constants of BNPP hydrolysis by complex [Cu-$OH_2^{2+}$] and [Cu-$OH^+$], respectively , BNPP = bis(*p*-nitrophenyl)phosphate))**

The low activity of these catalysts towards phosphate ester hydrolysis may be disadvantageous for their use in mechanocatalysis, due to the short lifetime of a mechanically activated catalyst. Therefore other reactions can be investigated, such as the hydrolysis of *p*-nitrophenylacetate (*p*NPA). This substrate has been widely used in the elucidation of the mechanism of action of chymotrypsin and other enzyme mimics.[98] Moreover, Hegg and Burstyn have reported a TMTACN – copper derivatized complex that is able to cleave an unactivated peptide bond,[99] which is remarkable considering the great stability of amide bonds.[100] This example shows that TMTACN-copper can catalyze a versatility of hydrolyzable substrates.

## 4.2 Results and discussion of kinetic studies on the TMTACN – Cu model system

*p*-Nitrophenyl esters are frequently used substrates in kinetic studies of enzymes and synthetic mimics, because the formation of *p*-nitrophenol can be easily detected by UV-Vis spectroscopy. At room temperature *p*-nitrophenol has a pKa of 7.16; this implies that at neutral conditions both *p*-nitrophenol and *p*-nitrophenolate will be present. The anionic species exhibits a strong absorption at λ = 400 nm (ε = 11 800 $M^{-1}$ $cm^{-1}$) while at the same wavelength the neutral compound show a very weak absorption (ε = 2000 $M^{-1}$ $cm^{-1}$).[101] A good measure for the conversion of *p*-nitrophenyl ester into its hydrolyzed product at neutral conditions is to record the absorption at the isobestic point (λ = 348 nm) for *p*-nitrophenol and *p*-nitrophenolate formation. At high pH, the production of *p*-nitrophenolate can be monitored by measuring the absorbance at λ = 400 nm.

### 4.2.1 Hydrolysis of *p*-nitrophenylacetate (*p*NPA)

In general, esters can be hydrolyzed under basic and acidic conditions.[100] It is expected that esters are relatively stable at neutral pH. In case of *p*NPA, the electron withdrawing para-nitrophenyl group makes the ester more prone to hydrolysis. The spontaneous hydrolysis of *p*NPA will therefore be substantial.

It is plausible that *p*NPA will show a similar behavior upon hydrolysis as the BNPP substrate. It is expected that hydrolysis of *p*NPA starts by the coordination of substrate to the metal center. Upon intramolecular attack of the hydroxide to the ester, the ester is hydrolyzed and *p*-nitrophenol is released. The total reaction of the hydrolysis of *p*NPA can be described as the sum of the spontaneous hydrolysis and the metal catalyzed hydrolysis (4.1)

$$\text{Rate of reaction} = k_0\,[p\text{NPA}] + k_c\,[\text{cat}][p\text{NPA}] \qquad (4.1)$$

In which $k_0$ = rate constant of the spontaneous hydrolysis reaction, $k_c$ = rate constant of the hydrolysis reaction by the catalyst, [*p*NPA] = concentration of *p*-nitrophenylacetate and [cat] = concentration of the catalyst.

Initial rate kinetics can be used to deduce the observed rate constant, which can be calculated by the change of absorption at the isobestic point over time. To investigate the catalytic behavior of the mononuclear diaqua complex **[L1Cu($H_2O$)$_2$]** and the dimeric oxalate bridged copper complex **[L1Cu-μ-Ox]**, the complexes were dissolved in a pH 7 buffer solution together with *p*NPA. Using a substrate to catalyst ratio = 16 (**[L1Cu($H_2O$)$_2$]** , **[L1Cu-μ-Ox]** = 0.125 mM; [*p*NPA] = 2 mM) and buffer pH 7 ((50 mM); Ionic strength (I) = 0.1 M) UV-Vis spectra were recorded every 10 min over a period of 180 min. As control, the reaction was also carried out without the addition of catalyst (Table 4.1).

**Table 4.1 Observed rate constants of TMTACN Cu complexes discussed in this study.**

| Complex | $k_{obs}$ ($s^{-1}$) |
|---|---|
| **[L1Cu($H_2O$)$_2$]** | $3.60 \times 10^{-4}$ |
| **[L1Cu-μ-Ox]** | $2.47 \times 10^{-4}$ |
| **Control** | $2.07 \times 10^{-4}$ |

The control experiment showed a linear relationship of *p*-nitrophenol (NP) production over time (Figure 4.1), which is related to the spontaneous hydrolysis of *p*NPA. The oxalate bridged **[L1Cu-μ-Ox]** complex shows a slight increase in the rate of reaction. We expected that the oxalate bridged complex to be inactive in the hydrolysis reaction, and therefore it should show a similar rate constant as the control experiment. The unexpected observation may be due to competitive binding of the substrate with oxalate. The reported association constants of oxalate-copper binding in similar systems are high, that reaches up to $10^5$ $M^{-1}$. The association constant of the *p*-nitrophenylacetate with copper is not reported. Because the concentrations of copper oxalate complexes are low, there may be (a substantial amount of) mononuclear copper species in solution present, which these can interact with the substrate that is in large excess. Hydrolysis of the substrate leads therefor to an increased rate constant. The mononuclear copper **[L1Cu($H_2O$)$_2$]** complex shows a larger rate enhancement as compared to **[L1Cu-μ-Ox]** and the control experiment. The hydrolysis rate is fast at the initial phase (0-20 min) of the experiment. (Figure 4.1) This kind of behavior is also observed by enzymes, and is denoted as the so-called burst phase. At the initial period of the reaction, product formation will be high until saturation of substrate on the catalyst is achieved.

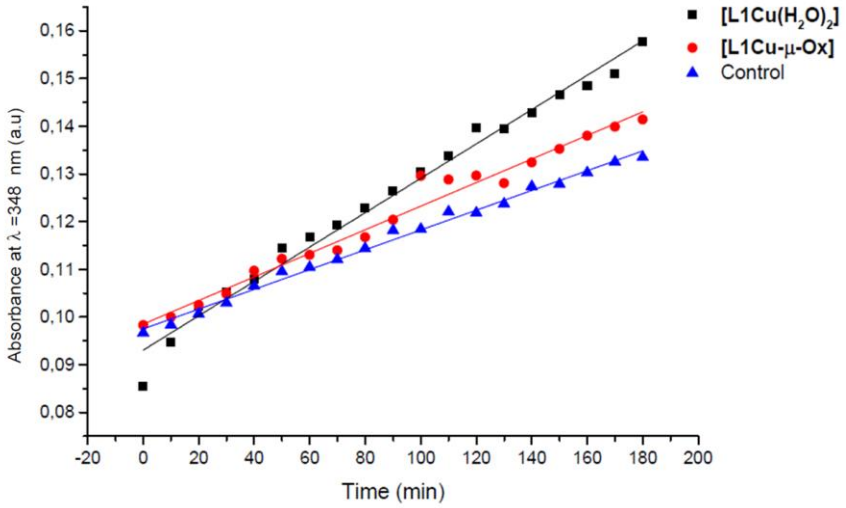


**Figure 4.1 Hydrolysis of *p*NPA under neutral conditions; time progress curves of the absorbance at λ = 348 nm for the [L1Cu($H_2O$)$_2$] and [L1Cu-μ-Ox] complexes and the control.**

This experiment shows that the mononuclear complex is active in the hydrolysis of *p*NPA, but it also shows that the oxalate bridged complex is unstable in dilute solutions and may dissociate into an active specie. Moreover, the deviation in the rate of reaction with the background reaction (that is the spontaneous hydrolysis) is small. This can cause difficulty in distinguishing the hydrolysis reaction catalyzed by the mechanically activated catalyst from the background reaction, considering that in reported examples of mechanocatalysts the amount activated catalyst is low. Therfore, we investigated the conditions in which the difference of the background reaction and the copper catalyzed reaction could be further increased.

At first, the hydrolysis reaction of *p*NPA using **[L1Cu($H_2O$)$_2$]** complex was tested using a pH 9 buffer, instead of pH 7. Under these basic conditions the deprotonation of the coordinated water will occur, which will enhance the reactivity of the hydrolysis reaction. Unfortunately, apart from the increase in activity of the copper catalyzed reaction, the background reaction showed an increase in reaction rate too (Figure 4.2).

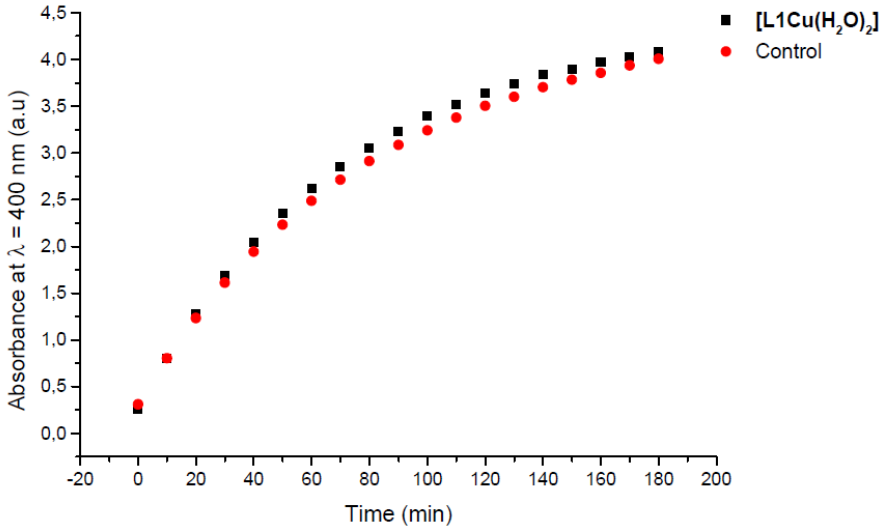


**Figure 4.2 Hydrolysis of *p*NPA under basic conditions; time progress curves of the absorbance at λ = 400 nm for the [L1Cu(H$_2$O)$_2$] complex and the control.**

We therefore decided to investigate other substrates that might give a clear difference in the reaction rates of the (active) **[L1Cu(H$_2$O)$_2$]** complex, the (inactive) oxalate **[L1Cu-μ-Ox]** complex and (inactive) control experiment.

### 4.2.2 Hydrolysis of bis-(*p*-nitrophenyl)phosphate (BNPP)

The use of BNPP, which has a low spontaneous hydrolysis rate at neutral conditions, in the study of the catalytic activity of the TMTACN based oxalate bridged complex may be a more appropriate substrate.[102] In this experiment a large excess of the copper complex is used as compared to the experiments of *p*NPA hydrolysis, in which a ratio of substrate/catalyst = 16 was employed. We believed that in case of the low concentration of dimeric copper oxalate complexes with respect to the substrate concentration, a substantial amount of dissociated copper complexes will be present, to which the substrate can coordinate and that can lead to substrate hydrolysis. To verify this, we conduct this experiment in excess of catalyst. In this way the activity of the oxalate bridged complex can be evaluated and will therefore not be influenced by other factors, such as dissociation in dilute solutions.

The reaction of the catalyzed reaction of hydrolysis of BNPP can be described as the sum of the hydrolysis of BNPP and NPP:

$$\text{Rate of reaction} = k_1\,[\text{cat}][\text{BNPP}] + k_2\,[\text{cat}][\text{NPP}] \qquad (4.2)$$

in which $k_1$ , $k_2$ = rate constants of BNPP and NPP hydrolysis reaction, respectively; [cat] = catalyst concentration;[BNPP] = bis(*p*-nitrophenyl)phosphate concentration; [NPP] = concentration of *p*-nitrophenylphosphate.

Because the catalyst concentration is in excess, it can be treated as a constant, and described as a pseudo-first order reaction (4.3).

$$\text{Rate of reaction} = k_{obs1}\,[\text{BNPP}] + k_{obs2}\,[\text{NPP}] \qquad (4.3)$$

In which $k_{obs1}$ and $k_{obs2}$ are the observed rate constants in the hydrolysis of BNPP and NPP, respectively; [BNPP] = bis(*p*-nitrophenyl)phosphate concentration and [NPP] = concentration of *p*-nitrophenylphosphate.

Upon fitting the data with an exponential function

$$y = A + B\exp(-k_{obs1}\,t) + C\exp(-k_{obs2}\,t) \qquad (4.4)$$

the observed rate constants can be calculated. To investigate the catalytic behavior of the mononuclear diaqua complex **[L1Cu($H_2O$)$_2$]** and the dimeric oxalate bridged copper complex **[L1Cu-μ-Ox]**, the complexes were dissolved in a pH 9 buffer solution together with BNPP. Using a substrate to catalyst ratio = 0.015 (**[L1Cu($H_2O$)$_2$]** , **[L1Cu-μ-Ox]** = 1 mM; [*p*NPA] = 0.015 mM) and buffer pH 9 ((0.1 M); Ionic strength (I) = 0.3 M) UV-Vis spectra were recorded every 10 min over a period of 250 min. As control, the reaction was also carried out without the addition of catalyst (Table 4.1). As control, the reaction was also carried out without the addition of catalyst.

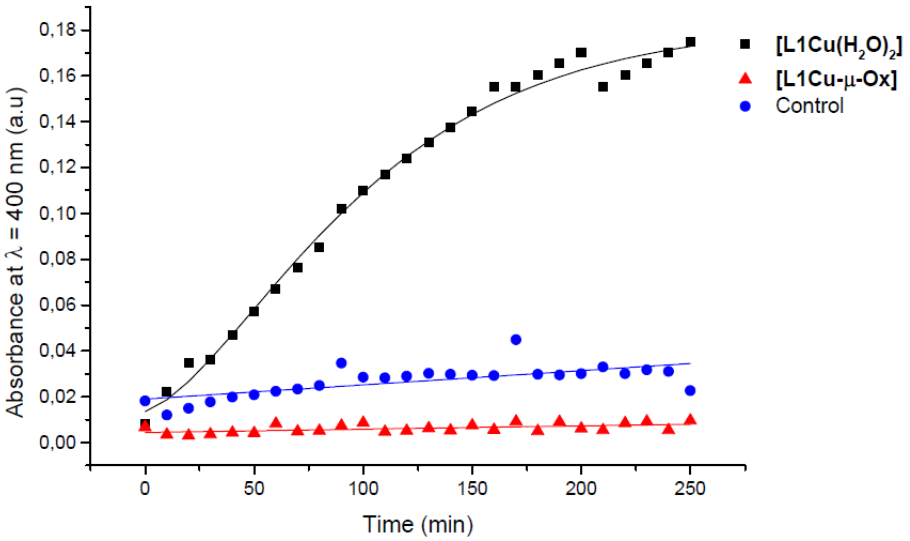


**Figure 4.3 Hydrolysis of BNPP under basic conditions; time progress curves of the absorbance at λ = 400 nm for the [L1Cu($H_2O$)$_2$] and [L1Cu-μ-Ox] complexes and the control.**

The obtained data could be readily fitted using equation (4.4). Resulting in $k_{obs1}$ = 3.3 $10^{-4}$ and $k_{obs2}$ = 2.6 $10^{-4}$ $s^{-1}$, which are in relatively the same orders as compared to the reported value of $k_{obs1}$ = 6.0 $10^{-5}$ $s^{-1}$ (values of $k_{obs2}$ were not reported). From Figure 4.3 can be seen that the [**L1Cu($H_2O$)$_2$]** showed a clear activity towards BNPP hydrolysis and both control and the oxalate **[L1Cu-μ-Ox]** complex showed no indication of NP formation (Figure 4.3). This observation may suggest that in dilute solution, a substantial amount of the dissociated form is present, while at higher concentration the amount of mononuclear copper species is minimal.

## 4.3 Conclusion

The investigation on the activity towards the hydrolysis of ester by the oxalate bridged **[L1Cu-μ-Ox]** complex lead to unambiguous results. It is observed that at low complex concentrations the complex is active in the hydrolysis of *p*NPA, while at high concentrations this did not show any activity in the hydrolysis of BNPP. In dilute solutions the copper oxalate complex may exist in the dissociated form and upon the binding of the substrate to copper leads to activity in the hydrolysis reaction. In the BNPP hydrolysis reaction, the difference in the rate of NP formation between metal catalyzed reaction and the control reaction was of sufficient difference as compared to the hydrolysis of *p*NPA. The metal catalyzed reaction showed to be active in the BNPP hydrolysis reaction, while the control reaction did not show any activity. Moreover, it has been shown that hydrolysis of BNPP will not occur when **[L1Cu-μ-Ox]** is added.

## 4.4 Experimental section

Instrumentation:

All UV-Visible spectra and kinetic runs were performed using 1 cm cuvettes on a Cary 300 UV-Vis which was equipped with a cell holder whose temperature can be regulated via an external circulating water bath (Varian). The pH was measured with a Consort C931 pH meter.

Preparation of stock solutions:

Buffer solutions with pH = 7 and 9 with constant ionic strength (I) of 0.3 M (Buffer pH7A, pH9A) and 0.15 M (Buffer pH7B, pH9B) ($NaClO_4$) and a concentration of 0.1 M and 0.05 M, respectively, were prepared as described in Appendix D. The following buffers were used: 3-morpholinopropane-1-sulfonic acid (MOPS) (pH 7.4) and 2-(Cyclohexylamino)ethanesulfonic acid (CHES) (pH 8.8). Aqueous stock solutions of **[L1Cu-($H_2O$)$_2$]** and **[L1Cu-μ-Ox]** (10 mM) and BNPP (45 μM), pNPA (8.3 mM) were freshly prepared for each kinetic experiment.

Kinetic studies:

Hydrolysis of *p*NPA, to 1.5 mL of buffer pH7B or pH9B, 37.5 µL of **[L1Cu-($H_2O$)$_2$]** and **[L1Cu-µ-Ox]**-stock solution and 739 µL $H_2O$ were added in the cuvette. This was placed in the cell block of the spectrophotometer and this was stirred for 10 min while the temperature was allowed to equilibrate. Then, 722 µL of *p*NPA stock solution was added to the stirring solution and the temperature was allowed to equilibrate for a further 2 min. After this time the measurement was started by monitoring the NP formation at λ = 348 nm over a period of 180 min (with readings taken at a 10 min interval).

For the hydrolysis of BNPP, a similar procedure as for the hydrolysis of *p*NPA was used, with the exception that 1.5 mL of buffer pH9A, 0.3 mL of **[L1Cu-($H_2O$)$_2$]** and **[L1Cu-µ-Ox]**-stock solution and 0.2 mL $H_2O$ and 1 mL of BNPP stock solution was used. NP formation was monitored at λ = 400 nm over a period of 250 min (with readings taken at a 10 min interval).

# Chapter 5 Solvent swelling studies on poly(2-hydroxyethylmethacrylate) films incorporated with [L2Cu-μ-Ox]

## 5.1 Introduction

In previous chapters the synthesis of polymerizable TMTACN ligands, its formation into a copper complex and its catalytic activity towards ester hydrolysis was reported. In this chapter the incorporation of the polymerizable copper complex in a polymer network that is, preferably, compatible with an aqueous environment required for the hydrolysis of BNPP, is described. Furthemore, the preliminary results on the catalytic behavior of the films are reported.

### 5.1.1 Solvent swelling in mechanochemistry

Earlier studies on a spiropyran mechanophore showed that a spiropyran (SP) can undergo electrocyclic ring opening to the fluorescent merocyanine (MS) dye under mechanical force.[36] Related to this, the group of Moore has recently reported activation of a spiropyran mechanophore, that is cross-linked in a poly(methyl methacrylate) network, induced by solvent swelling.[103] (Figure 5.1) They observed a correlation in the degree of swelling and fluorescence intensity, which implies that the forces generated by solvent swelling are the driving force for the activation of SP into the fluorescent MC form. Inspired by this work, we investigated the activation of our TMTACN-copper based (mechano)catalyst by solvent swelling.

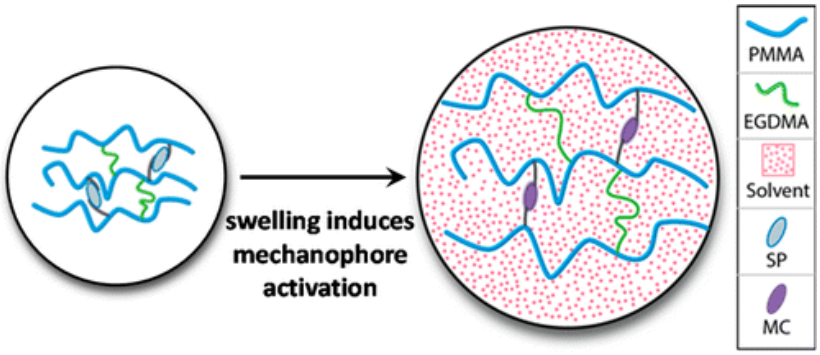


**Figure 5.1 Schematic overview on the solvent swelling induced mechanophore activation.**

### 5.1.2 Development of a poly(hydroxyethyl)methacrylate based TMTACN-copper catalyst

As already mentioned the catalyst should be incorporated in a hydrophilic scaffold and, moreover, water is required to swell the polymer. Therefore, the hydrophilic monomer, 2-

hydroxyethylmethacrylate (HEMA), was used to form a polymer network. The synthesized polymerizable complexes **[L2Cu-μ-Ox]** can act as a crosslinking agent due to the two methacrylate groups present on each end of the complex. Co-polymerization of **[L2Cu-μ-Ox]** with HEMA will hopefully result in the formation of a network with a highly hydrophilic character. The HEMA based polymer (pHEMA) can be swelled in water to form a hydrogel, which the water uptake is partly dependent on the degree of crosslinking and flexibility of the crosslinker.[104] It was found that degree of swelling with a more flexible polyethelene glycol dicacrylate (PEGDA) crosslinker was more enhanced as compared to a rigid ethylene glycol diacrylate (EDGA). We have, therefore, chosen tetraethylene glycol diacrylate (TEGDA) as co-crosslinker along with the polymerizable copper complex. In this way a certain degree of crosslinking is obtained, which is needed to transduce macroscopic force to the mechanocatalyst via chemical – or physical crosslinks.[105] (Scheme 5.1)

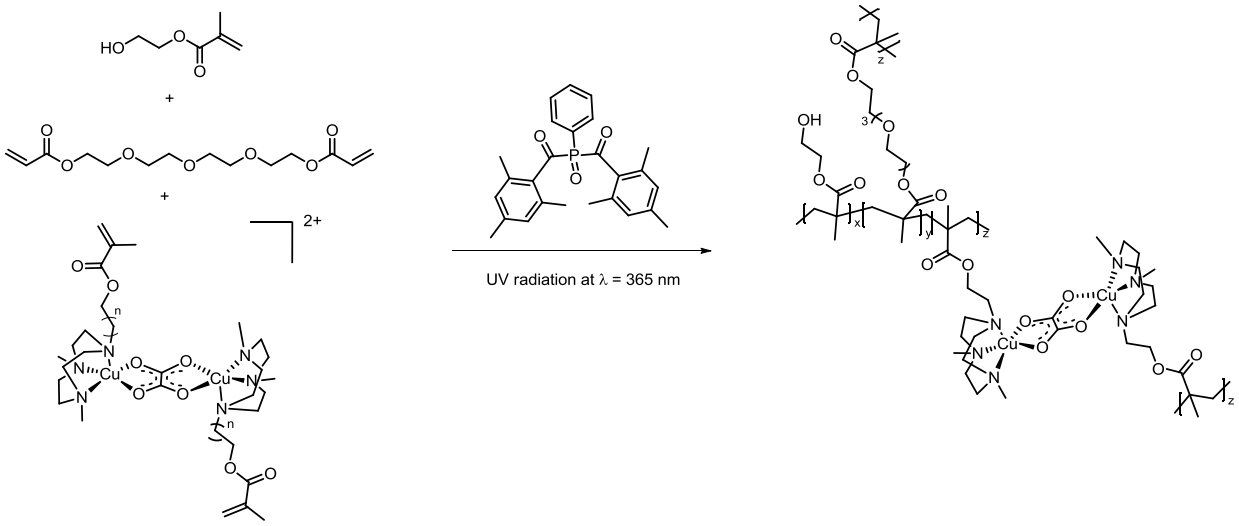


**Scheme 5.1 Synthetic scheme of [L2Cu-μ-Ox] based pHEMA films with a TEGDA crosslinker.**

## 5.2 Synthesis of a TMTACN-copper derivatized mechanocatalyst

Crosslinked pHEMA films with varying copper catalyst concentration can be prepared by UV-initiated free radical polymerization. At first, acetonitrile solutions of phenylbis(2,4,6-trimethyl)benzoylphosphine oxide photoinitiator, the dinuclear oxalate bridged copper **[L2Cu-μ-Ox]** complex, TEGDA crosslinker and HEMA monomer were prepared. (Table 5.1) Upon evaporation of the solvent a homogeneous solution was obtained for the samples which had a low **[L2Cu-μ-Ox]** concentrations (0.01 – 0.05 mol%). For the highest concentration of copper complex (0.1 mol%), phase separation occurred upon mixing as could be seen by a blue solid, indicating the **[L2Cu-μ-Ox]** complex**,** present in solution.

**Table 5.1 Preparation of pHEMA films with different compositions of [L2Cu-μ-Ox] and TEDGA**

| Film | [L2Cu-μ-Ox] (mol%) | TEGDA (mol%) | Total crosslink (mol%) | Photoinitator (wt%) |
|---|---|---|---|---|
| **pHEMA-Cu1** | 0.1 | 0.9 | 1 | 0.5 |
| **pHEMA-Cu2** | 0.05 | 0.95 | 1 | 0.5 |
| **pHEMA-Cu3** | 0.01 | 0.99 | 1 | 0.5 |
| **pHEMA-Control** | 0 | 1 | 1 | 0.5 |

The solution was dropped on top of a glass substrate and polymerization on the glass substrate was carried out upon irradiation of UV light at λ = 365 nm for 10 minutes under a $N_2$ flow. This resulted in highly transparent glassy polymers, except for the **pHEMA-Cu1** film in which blue particles were observed in the polymer film, (Figure 5.2) attached to the glass substrate.

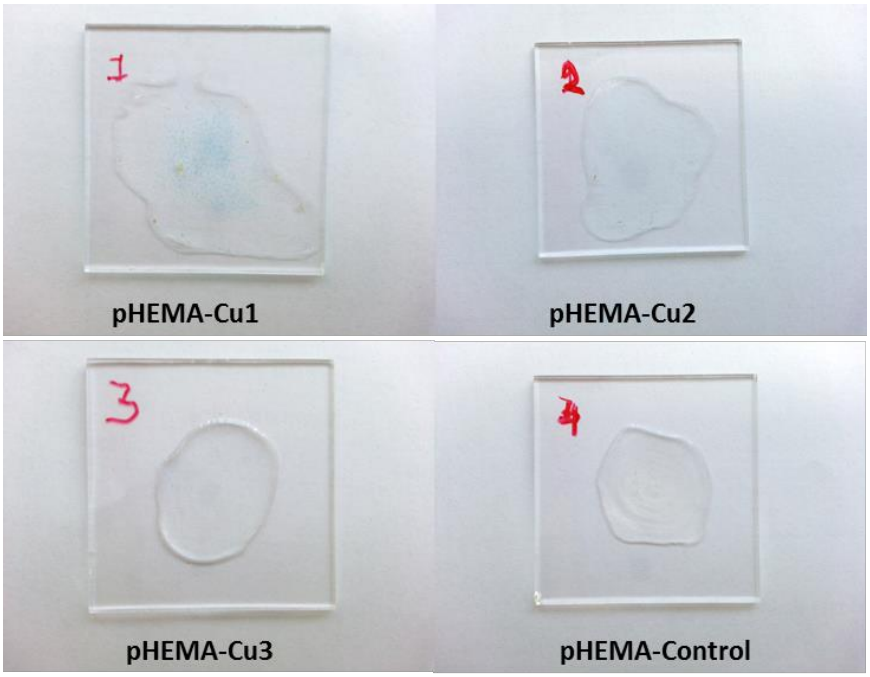


**Figure 5.2 pHEMA films after UV radiation; a blue solid is observed for the pHEMA-Cu1 film; other pHEMA films are transparent.**

### 5.2.1 Characterization of the polymer films

Infrared spectroscopy can be used to characterize the polymer films. As described previously, the copper complexes were also characterized by IR since the vibrational bands of the oxalate and the

carbonyl stretches of the methacrylate ester can be clearly observed. The polymer films should therefore also exhibit these characteristic bands.

However, due to the low complex concentrations in the polymer films, incorporation of the copper oxalate bridged complex was difficult to verify. A weak band at 1636 $cm^{-1}$, which we attribute to the C=O stretching mode of the oxalate group was observed for all the polymer films with the copper oxalate complex, except for the **pHEMA-Cu3** film this band was almost not observable, due to the very low concentration of copper complex. Importantly, this vibrational band was not observed for the **pHEMA-Control** film (Figure 5.3). This suggests that the copper oxalate complex is incorporated into the polymer network. A weak band at 814 $cm^{-1}$ that correspond to the C=C stretch of the methacrylate was observed, which points out that full conversion of the polymerization was not achieved.

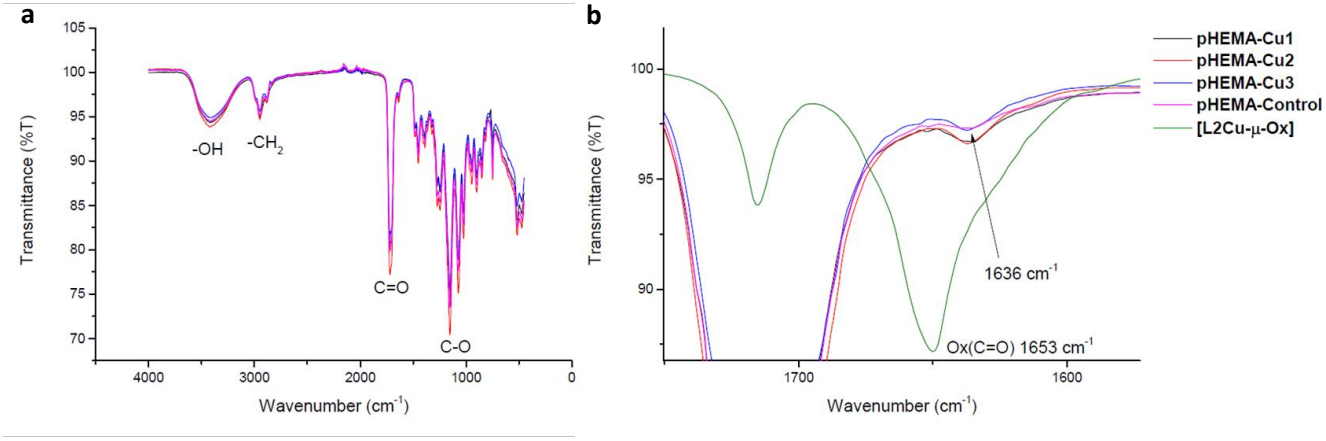


**Figure 5.3 IR spectra of the synthesized polymers. (a) The characteristic bands of the HEMA monomer and TEGDA crosslinker. (b) A weak band that refers to the C=O stretch at 1636 $cm^{-1}$ was observed for the polymers with [L2Cu-μ-Ox] complex**

## 5.3 Solvent swelling of polymer network with [L2Cu-μ-Ox]

After incorporation of the oxalate bridged copper complex **[L2Cu-μ-Ox]** in a pHEMA network, we studied the swelling induced activation of this dormant, inactive catalyst. To this end, **pHEMA-Cu1-3** and the **pHEMA-Control** films were swollen in a 1 mM BNPP pH buffered solution by placing the polymer film, which is attached on the glass substrate, in a petri dish containing the buffer solution and placed in oven at 50 °C. Since this is not a closed system, solvent evaporated during the time period. This leads to the decrease in volume of the solutions, and the concentrations are increased. Because this effect can be different for each sample, a good comparison of results between the samples could not be made.

In order to improve the swelling conditions, polymer films on a smaller glass substrate were prepared which could fit in a closed vial (Table 5.2).

**Table 5.2 Preparation of pHEMA films with different compositions of [L2Cu-μ-Ox], TEDGA and photoinitiator.**

| Film | [L2Cu-μ-Ox] (mol%) | TEGDA (mol%) | Total crosslink (mol%) | Photoinitator (wt%) |
|---|---|---|---|---|
| **pHEMA-Cu4** | 0.05 | 0.95 | 1 | 0.1 |
| **pHEMA-Cu5** | 0.01 | 0.99 | 1 | 0.1 |
| **pHEMA-Cu6** | 0.05 | 0.95 | 1 | 0.5 |
| **pHEMA-Cu7** | 0.01 | 0.99 | 1 | 0.5 |
| **pHEMA-control2** | 0 | 1 | 1 | 0.1 |
| **pHEMA-control3** | 0 | 1 | 1 | 0.5 |

The volumes of these BNPP solutions were chosen in such a way that the effective copper concentration was 5 μM for all polymer films. The polymer films were placed in a buffered BNPP solution as described above. During the experiment, the degree of swelling and absorption at λ = 400 nm, that indicate the formation of *p*-nitrophenol (NP) formation, were measured. The degree of swelling is defined as:

$$\text{Degree of swelling (\%)} = ((m - m_0) / m_0) \times 100\% \qquad (5.1)$$

Where m is the mass of the swollen polymer and $m_0$ is the mass of the dry polymer. In Table 5.3 the degree of swelling and the turnover number (TON) after 41 h are summarized. In this study a longer experimental time is covered as compared to the kinetic studies outlined in chapter 4, because the formation of NP is low in the initial phase of the experiment. All polymers exhibited a similar degree of swelling. Furthermore, no significant trend in swelling degree was observed between the amount of the copper complex crosslinking or initiator concentration. Table 5.3 shows that with increasing initiator concentration, the turnover number is decreased. This might be explained by the fact that at high initiator concentrations, the polymers consist of relatively short chains which might influences the force transduction to the copper oxalate complex.

**Table 5.3 The degree of swelling and the TON measured after 41 h.**

| Film | Swelling degree (%) | Turnover number (TON)* after 41 h |
|---|---|---|
| **pHEMA-Cu4** | 100 | 2.7 |
| **pHEMA-Cu6** | 126 | 2.6 |
| **pHEMA-Cu7** | 107 | 1.8 |
| **pHEMA-Cu8** | 132 | 1.8 |
| **pHEMA-Control2** | 77 | - |
| **pHEMA-Control3** | 107 | - |

* = TON is defined as concentration NP / concentration of effective copper concentration (unitless)

The relation between the amount of swelling and the conversion of BNPP into NP, measured at λ = 400 nm, is depicted in Figure 5.4. A clear difference in BNPP hydrolysis between the copper containing pHEMA (Figure 5.4 a-d) and the control films (Figure 5.4e and f) can be observed. The increasing release of NP, that is an increasing absorption at λ = 400 nm, indicates that the **pHEMA-Cu4-7** films are active catalysts for the hydrolysis reaction. In contrast, the control films do not show an increase of the signal at λ = 400 nm indicating that no NP is formed. It is expected that forces generated by solvent swelling correlates to the quantity of activated catalyst and therefor the conversion. Although, the swelling of pHEMA-Cu4-7 the absorbance λ = 400 nm increased, no direct correlation between the amount of swelling % and increase in absorption was observed.

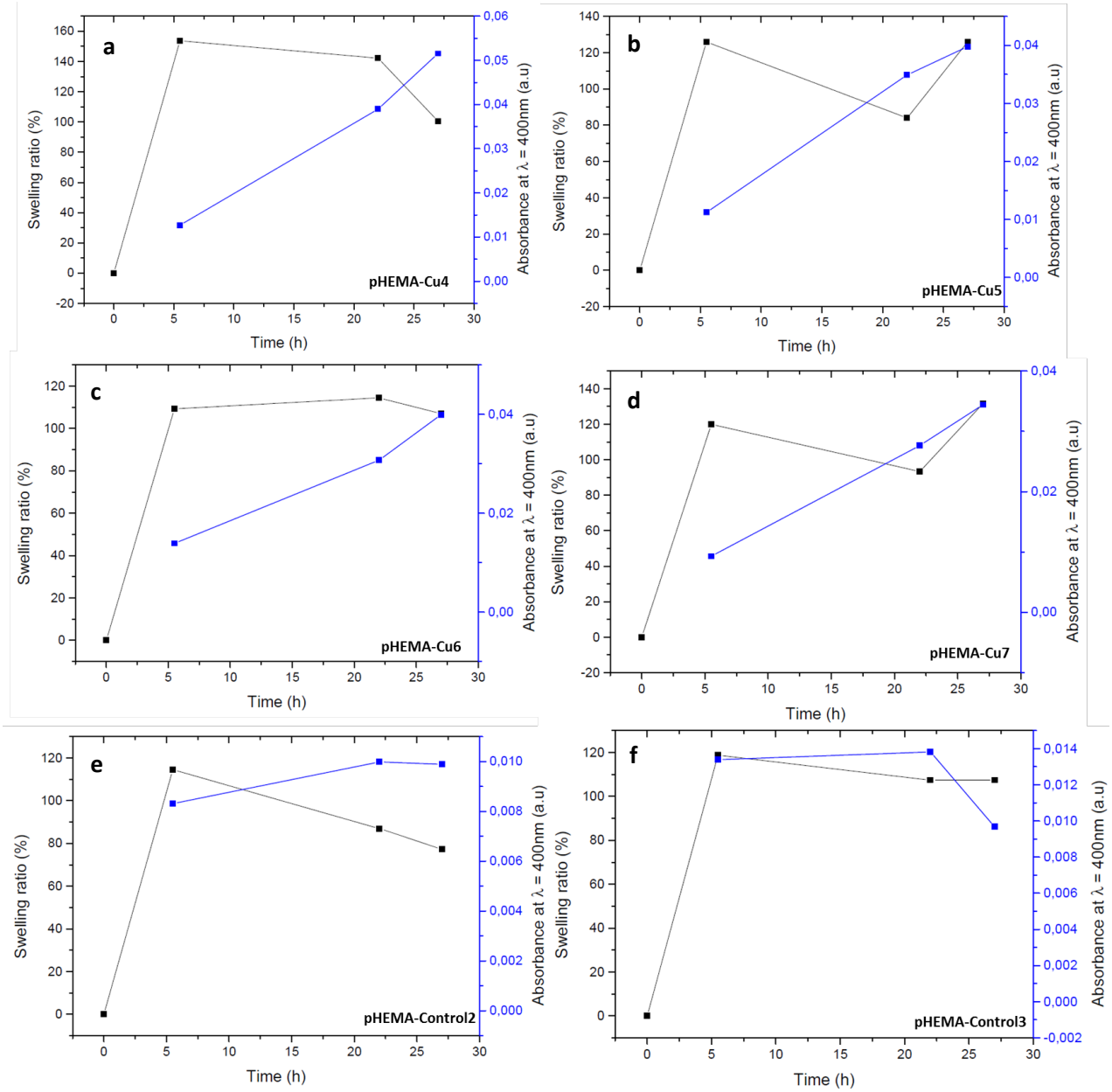


**Figure 5.4 Degree of swelling (black) and absorbance at λ = 400 nm (blue) over time. a-d) pHEMA films with copper oxalate complex incorporated (pHEMA-Cu4-7) and e-f films without the complex (pHEMA-Control2-3). The films are swollen in a buffered BNPP solution at 50 °C. Note that the swelling ratios fluctuate; these measurements should be repeated to be able to explain if the fluctuations are significant.**

In a control experiment, **[L2Cu-μ-Ox]** was dissolved, with the same copper complex concentration as the polymer films, in a BNPP solution and the NP formation was monitored by UV-Vis spectroscopy. This control experiment is carried out, because the hydrolysis reaction studied in chapter 4 was performed under different conditions (experiment time and substrate/catalyst ratio) as compared to the swelling studies. Kinetic studies outlined in chapter 4 used an excess of the copper oxalate complex (1 mM) and the substrate concentration was held at 15 μM. In this experiment, the concentrations are reversed, that is, the substrate concentration (1 mM) is in excess and the amount of the copper complex is low. As can be seen from Figure 5.5, catalytic activity is observed, indicating

that the binuclear oxalate bridged complex is not stable in its dimeric form at low concentration with an excess of BNPP. The TON of this catalyst reaches 1.3 after 41 h. This is lower as compared to the activated copper complexes in the pHEMA films.

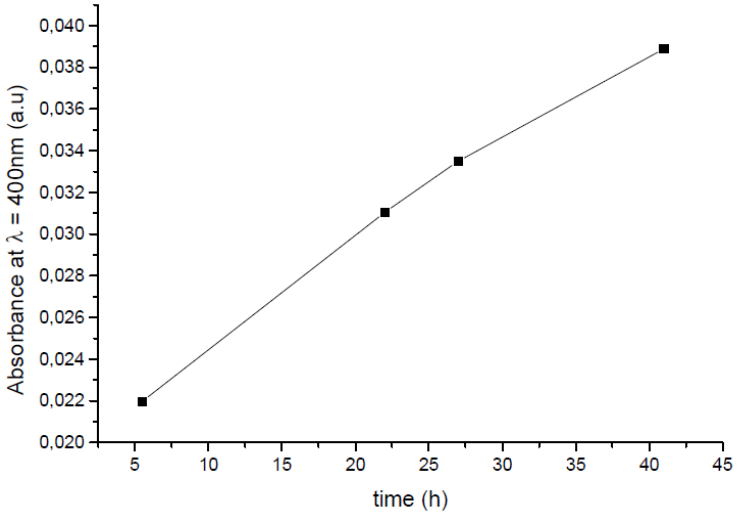


**Figure 5.5 Absorbance at λ = 400 nm for the [L2Cu-μ-Ox] complex dissolved in a buffered BNPP solution at 50 °C over time.**

Taken the experiments above into account, it is difficult to conclude whether the catalysis is activated by solvent swelling. Additional control experiments should be performed to exclude the competitive BNPP binding, which can be done by treating the polymeric films with a low concentration of BNPP instead of an excess. Moreover, it is important to investigate solvent swelling on a mononuclear copper oxalate complex, which can in principle not be mechanically activated, as a control experiment. In this way, a better understanding on the swelling induced catalyst activation can be obtained.

## 5.4 Conclusion

The copper complex **[L2Cu-μ-Ox]** was incorporated in a pHEMA network as confirmed by characterization with IR spectroscopy. The **pHEMA-Cu4-7** films showed activity in the hydrolysis reaction, in contrast to the films without the catalyst. In a control experiment, a copper oxalate complex was dissolved in solution showed that this was active in the hydrolysis reaction, although, with a lower turnover number. To conclude, swelling studies on these polymer films did not lead to conclusive results, as there are many uncertainties that should be investigated more thoroughly. The polymer films with copper oxalate complex incorporated do, however, show catalytic activity in the hydrolysis of BNPP.

## 5.5 Experimental section

General:

All UV-Visible measurements were performed using 3 mm cuvettes on a Cary 300 UV-Vis which was equipped with a cell holder whose temperature can be regulated via an external circulating water bath (Varian). The pH was measured with a Consort C931 pH meter.

**General procedure for the synthesis of pHEMA films**

Stock solutions of 10 mg/mL in MeCN for the phenylbis(2,4,6-trimethyl)benzoylphosphine oxide photoinitiator and TEGDA and 5 mg/mL for **[L2Cu-μ-Ox]** in MeCN were used.

Depending on the wt% or mol% of initiator and crosslinker, an amount of the stock solution was mixed with HEMA (0.5 mL) (Appendix E). To this, 1 mL of MeCN was added to obtain a homogeneous solution and the solvent was evaporated to yield a clear solution. The polymer solution was dropped on a glass substrate, which was cleaned thoroughly with acetone and ethanol before use. The substrate was irradiated at λ = 365 nm using UV light for 10 minutes at room temperature under a $N_2$ flow. Highly transparent, glassy polymer films were obtained.

**General procedure on the swelling of pHEMA films**

Stock solutions:

An aqueous solution of BNPP (10 mM) was used. Buffer pH 9 solution of 0.1 mM with an ionic strength of 0.3 mM was prepared as described in Appendix D.

Polymer film swelling:

The pHEMA films were placed in a vial and Buffer pH 9, BNPP solution and water were added to this vial (Appendix E). The vial was closed with a cap and sealed to prevent possible evaporation. The vials were placed in an oven at 50 °C. And certain time intervals the vials were taken out of the oven and the mass of the polymers were measured. Also the UV-Vis spectrum of the BNPP solutions was directly (without dilution) recorded.

## Conclusions and Outlook

The aim of this project was to investigate the mechanical activation of a TMTACN-copper(II) based catalyst to broaden the scope of mechanocatalysts. A requisite for the activation of a mechanocatalyst is the transduction of macroscopic force to the metal-ligand bond to cause bond scission. The catalyst should be therefore in a dormant, inactive state before the force is applied.

The transduction of force to the metal-ligand bond can be achieved by attachment of polymers on the ligands that are complexed to a metal center. Therefore, the TMTACN derivative should be functionalized with a polymerizable group. Conversion of 1,4-dimethyl-1,4,7-triazacyclononane proved to be difficult and did not lead to a derivative to which a polymerizable group could be attached. However, the synthesis of the polymerizable ligand was proven to be successful when a functional pendant arm was directly incorporated in the triazacyclononane macrocycle.

In order to stabilize the dimeric, inactive structure of the copper catalyst oxalate bridged copper complexes with the polymerizable ligands were synthesized and characterized by IR spectroscopy, UV-Vis-NIR spectroscopy and MALDI-TOF mass spectrometry. Moreover, model complexes consist of the active mononuclear diaqua -, the inactive dimeric di-μ-hydroxo - and the binuclear oxalate bridged TMTACN-copper(II) complexes were successfully synthesized and characterized.

An essential study toward the development of the mechanocatalyst is to investigate the catalytic activity of model complexes by the hydrolysis reaction on pNPA and BNPP substrates. It was found that the mononuclear diaqua **[L1Cu($H_2O$)$_2$]** complex is active in the hydrolysis reaction of pNPA and BNPP. The oxalate bridged **[L1Cu-μ-Ox]** complex showed to be instable upon dilution resulting in the hydrolysis of pNPA, while at high complex concentrations this did not show activity in BNPP hydrolysis. The hydrolysis without catalyst showed that pNPA is spontaneous hydrolyzed as for the BNPP substrate no formation of the hydrolyzed product was found.

And finally, upon the incorporation of the polymerizable copper complex in a pHEMA network, the mechanical activation by solvent swelling was investigated. Upon solvent swelling of the synthesized polymer films in a buffered BNPP solution at 50 °C, catalytic activity of the polymer films with the copper oxalate complex was observed. Additional control experiments should be performed to verify whether the activity is achieved by force induced by solvent swelling or it is influenced by other factors (such as the instability of the copper oxalate complex).

**Outlook**

At first the characterization of the incorporated copper complex films should be investigated in more detail. It was shown that only small changes are observable upon incorporation of low complex concentrations. Therefore, incorporation of higher concentrations of copper complex and washing of the polymer films might result in films that can be better characterized.

Experiments on catalyst activation on solvent swelling did not show conclusive results yet, as there are still many aspects to be investigated. Before this is studied, a more detailed investigation on the stability of the copper oxalate bridged should be performed. This can lead to optimization of the conditions in which the swelling studies are carried out.

And importantly, as a control experiment in the solvent swelling experiments, incorporation of a mononuclear copper oxalate complex in the pHEMA network should be investigated. This complex can in essence not be activated upon mechanical force, and therefore it shows whether the dormant, inactive oxalate bridged complex is activated upon solvent swelling of by other factors.

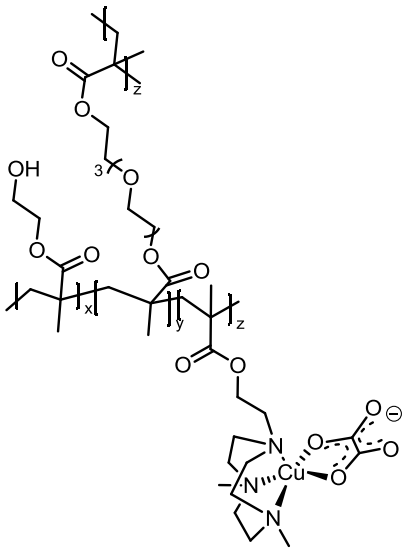


**Figure 6.1 Proposed mononuclear copper oxalate complex that can not be activated under mechanical force.**

## Acknowledgements

To begin with, I would like to thank my supervisor Erik, who guided and helped me throughout the project. I really learned a lot in terms of doing synthesis and even doing research in general. Moreover, I also would like to thank you for revising my thesis, which I imagine should be horrible (because of my somewhat weird use of English). I would like to thank Rint for giving me the opportunity for this master project. I appreciate the discussion moments with you, not only did you give very helpful suggestions but also you asked questions which led me to think about my research. I would like to thank dr. Pidko for taking place in the committee and reading my thesis. I hope to show you that organic synthesis can be fun too! I would like to thank the whole Sijbesma group in general; during the project I really enjoyed the nice work environment, and the suggestions/discussions during the weekly meetings were really insightful. To all of you good luck in the future! Particular thanks to Berry, for your help at the lab, with the polymerization of the films, UV –Vis meter, and for the nice discussions. Moreover I would like to thank all the students in STO3.43, you really provided a nice working atmosphere, also the discussions with you (not all related about chemistry) were nice to have.

Finally I want to thank my family, 多谢你们的照顾和支持， 如果没有你们，我不可能这么顺利度过这个实习时间。多谢阿妈，阿爸，慧贤， 永昕 和我最亲爱的嘉嘉！辛苦你们!

## References


(1) *IUPAC Compendium of Chemical Terminology: Gold Book*; Nič, M.; Jirát, J.; Košata, B.; Jenkins, A.; McNaught, A., Eds.; 2.1.0 ed.; IUPAC: Research Triagle Park, NC, 2009.

(2) Friščić, T.; Halasz, I.; Beldon, P. J.; Belenguer, A. M.; Adams, F.; Kimber, S. A. J.; Honkimäki, V.; Dinnebier, R. E. *Nat. Chem.* **2012**, *5*, 66–73.

(3) Kaupp, G. *CrystEngComm* **2009**, *11*, 388.

(4) James, S. L.; Adams, C. J.; Bolm, C.; Braga, D.; Collier, P.; Friščić, T.; Grepioni, F.; Harris, K. D. M.; Hyett, G.; Jones, W.; Krebs, A.; Mack, J.; Maini, L.; Orpen, A. G.; Parkin, I. P.; Shearouse, W. C.; Steed, J. W.; Waddell, D. C. *Chem. Soc. Rev.* **2012**, *41*, 413.

(5) Zhang, X.; Halvorsen, K.; Zhang, C.-Z.; Wong, W. P.; Springer, T. A. *Science* **2009**, *324*, 1330–1334.

(6) Staudinger, H.; Heuer, W. *Berichte Dtsch. Chem. Ges. B Ser.* **1934**, *67*, 1159–1164.

(7) Kauzmann, W.; Eyring, H. *J. Am. Chem. Soc.* **1940**, *62*, 3113–3125.

(8) Odell, J. A.; Keller, A. *J. Polym. Sci. Part B Polym. Phys.* **1986**, *24*, 1889–1916.

(9) *Macromolecules: Synthesis, Order and Advanced Properties*; Advances in Polymer Science; Springer-Verlag: Berlin/Heidelberg, 1992; Vol. 100/1.

(10) Kuijpers, M. W. A.; Iedema, P. D.; Kemmere, M. F.; Keurentjes, J. T. F. *Polymer* **2004**, *45*, 6461–6467.

(11) Odell, J. A.; Keller, A. *J. Polym. Sci. Part B Polym. Phys.* **1986**, *24*, 1889–1916.

(12) Odell, J. A.; Keller, A.; Muller, A. J. *Colloid Polym. Sci.* **1992**, *270*, 307–324.

(13) Larson, R. G. *Constitutive equations for polymer melts and solutions*; Butterworths series in chemical engineering; Butterworths: Boston, 1988.

(14) Porter, R. S.; Johnson, J. F. *J. Phys. Chem.* **1959**, *63*, 202–205.

(15) Price, G. J.; Smith, P. F. *Polymer* **1993**, *34*, 4111–4117.

(16) Groote, R. Mechanical activation of latent N-heterocyclic carbene catalysts.

(17) Hickenboth, C. R.; Moore, J. S.; White, S. R.; Sottos, N. R.; Baudry, J.; Wilson, S. R. *Nature* **2007**, *446*, 423–427.

(18) Ong, M. T.; Leiding, J.; Tao, H.; Virshup, A. M.; Martínez, T. J. *J. Am. Chem. Soc.* **2009**, *131*, 6377–6379.

(19) Caruso, M. M.; Davis, D. A.; Shen, Q.; Odom, S. A.; Sottos, N. R.; White, S. R.; Moore, J. S. *Chem. Rev.* **2009**, *109*, 5755–5798.

(20) Wiggins, K. M.; Brantley, J. N.; Bielawski, C. W. *Chem. Soc. Rev.* **2013**, *42*, 7130.

(21) Chen, Y.; Spiering, A. J. H.; Karthikeyan, S.; Peters, G. W. M.; Meijer, E. W.; Sijbesma, R. P. *Nat. Chem.* **2012**, *4*, 559–562.

(22) Davis, J. R. *Tensile testing*; ASM International: Materials Park, Ohio, 2004.

(23) Moses, D.; Feldblum, A.; Ehrenfreund, E.; Heeger, A.; Chung, T.; MacDiarmid, A. *Phys. Rev. B* **1982**, *26*, 3361–3369.

(24) Spain, I. L.; Dunstan, D. J. *J. Phys. [E]* **1989**, *22*, 923–933.

(25) Keller, A.; Odell, J. A. *Colloid Polym. Sci.* **1985**, *263*, 181–201.

(26) May, P. A.; Moore, J. S. *Chem. Soc. Rev.* **2013**, *42*, 7497.

(27) Lipatov, I. S.; Jennings, B. R.; Basedow, A. M. *Physical chemistry*; Springer-Verlag: Berlin; New York, 1977.

(28) Nguyen, T. Q.; Liang, Q. Z.; Kausch, H.-H. *Polymer* **1997**, *38*, 3783–3793.

(29) *Macromolecules: Synthesis, Order and Advanced Properties*; Advances in Polymer Science; Springer-Verlag: Berlin/Heidelberg, 1992; Vol. 100/1.

(30) Brantley, J. N.; Wiggins, K. M.; Bielawski, C. W. *Polym. Int.* **2013**, *62*, 2–12.

(31) Löwe, C.; Weder, C. *Adv. Mater.* **2002**, *14*, 1625–1629.

(32) Kim, S.-J.; Reneker, D. H. *Polym. Bull.* **1993**, *31*, 367–374.

(33) Nallicheri, R. A.; Rubner, M. F. *Macromolecules* **1991**, *24*, 517–525.
(34) Foulger, S. H.; Jiang, P.; Lattam, A. C.; Smith,, D. W.; Ballato, J. *Langmuir* **2001**, *17*, 6023–6026.
(35) Foulger, S. H.; Jiang, P.; Lattam, A.; Smith, D. W.; Ballato, J.; Dausch, D. E.; Grego, S.; Stoner, B. R. *Adv. Mater.* **2003**, *15*, 685–689.
(36) Davis, D. A.; Hamilton, A.; Yang, J.; Cremar, L. D.; Van Gough, D.; Potisek, S. L.; Ong, M. T.; Braun, P. V.; Martínez, T. J.; White, S. R.; Moore, J. S.; Sottos, N. R. *Nature* **2009**, *459*, 68–72.
(37) Youngblood, J. P.; Sottos, N. R. *Mrs Bull.* **2008**, *33*, 732–741.
(38) White, S. R.; Sottos, N. R.; Geubelle, P. H.; Moore, J. S.; Kessler, M. R.; Sriram, S. R.; Brown, E. N.; Viswanathan, S. *Nature* **2001**, *409*, 794–797.
(39) Cho, S. H.; White, S. R.; Braun, P. V. *Adv. Mater.* **2009**, *21*, 645–649.
(40) Kryger, M. J.; Ong, M. T.; Odom, S. A.; Sottos, N. R.; White, S. R.; Martinez, T. J.; Moore, J. S. *J. Am. Chem. Soc.* **2010**, *132*, 4558–4559.
(41) Klukovich, H. M.; Kean, Z. S.; Iacono, S. T.; Craig, S. L. *J. Am. Chem. Soc.* **2011**, *133*, 17882–17888.
(42) Paulusse, J. M. J.; Sijbesma, R. P. *Angew. Chem. Int. Ed.* **2004**, *43*, 4460–4462.
(43) Paulusse, J. M. J.; van Beek, D. J. M.; Sijbesma, R. P. *J. Am. Chem. Soc.* **2007**, *129*, 2392–2397.
(44) Paulusse, J. M. J.; Sijbesma, R. P. *Chem. Commun.* **2008**, 4416.
(45) Piermattei, A.; Karthikeyan, S.; Sijbesma, R. P. *Nat. Chem.* **2009**, *1*, 133–137.
(46) Tennyson, A. G.; Wiggins, K. M.; Bielawski, C. W. *J. Am. Chem. Soc.* **2010**, *132*, 16631–16636.
(47) Diesendruck, C. E.; Steinberg, B. D.; Sugai, N.; Silberstein, M. N.; Sottos, N. R.; White, S. R.; Braun, P. V.; Moore, J. S. *J. Am. Chem. Soc.* **2012**, *134*, 12446–12449.
(48) Jakobs, R. T. M.; Ma, S.; Sijbesma, R. P. *ACS Macro Lett.* **2013**, *2*, 613–616.
(49) Radzicka, A.; Wolfenden, R. *Science* **1995**, *267*, 90–93.
(50) Desbouis, D.; Troitsky, I. P.; Belousoff, M. J.; Spiccia, L.; Graham, B. *Coord. Chem. Rev.* **2012**, *256*, 897–937.
(51) Mildvan, A. S. *Proteins Struct. Funct. Genet.* **1997**, *29*, 401–416.
(52) Balaban, N. *Science* **1998**, *280*, 438–440.
(53) Chen, C.-A.; Cowan, J. A. *Chem. Commun.* **2002**, 196–197.
(54) Pyle, A. M.; Barton, J. K. In *Progress in Inorganic Chemistry*; Lippard, S. J., Ed.; John Wiley & Sons, Inc.: Hoboken, NJ, USA, 1990; Vol. 38, pp. 413–475.
(55) Klabunde, T.; Sträter, N.; Fröhlich, R.; Witzel, H.; Krebs, B. *J. Mol. Biol.* **1996**, *259*, 737–748.
(56) Huff, J. W.; Sastry, K. S.; Gordon, M. P.; Wacker, W. E. C. *Biochemistry (Mosc.)* **1964**, *3*, 501–506.
(57) Jones, D. R.; Lindoy, L. F.; Sargeson, A. M. *J. Am. Chem. Soc.* **1983**, *105*, 7327–7336.
(58) Morrow, J. R.; Trogler, W. C. *Inorg. Chem.* **1988**, *27*, 3387–3394.
(59) De Rosch, M. A.; Trogler, W. C. *Inorg. Chem.* **1990**, *29*, 2409–2416.
(60) Koike, T.; Kimura, E. *J. Am. Chem. Soc.* **1991**, *113*, 8935–8941.
(61) Burstyn, J. N.; Deal, K. A. *Inorg. Chem.* **1993**, *32*, 3585–3586.
(62) Deal, K. A.; Burstyn, J. N. *Inorg. Chem.* **1996**, *35*, 2792–2798.
(63) Deal, K. A.; Hengge, A. C.; Burstyn, J. N. *J. Am. Chem. Soc.* **1996**, *118*, 1713–1718.
(64) Hegg, E. L.; Burstyn, J. N. *Coord. Chem. Rev.* **1998**, *173*, 133–165.
(65) Deck, K. M.; Tseng, T. A.; Burstyn, J. N. *Inorg. Chem.* **2002**, *41*, 669–677.
(66) Fry, F. H.; Fischmann, A. J.; Belousoff, M. J.; Spiccia, L.; Brügger, J. *Inorg. Chem.* **2005**, *44*, 941–950.
(67) Chaudhuri, P.; Oder, K. *J. Chem. Soc. Dalton Trans.* **1990**, 1597.
(68) Madras, G.; Karmore, V. *Polym. Int.* **2001**, *50*, 683–687.
(69) Madras, G.; Chattopadhyay, S. *Polym. Degrad. Stab.* **2001**, *71*, 273–278.
(70) Price, G. J.; Smith, P. F. *Eur. Polym. J.* **1993**, *29*, 419–424.
(71) Peacock, D. H.; Gwan, Y. S. *J. Chem. Soc. Resumed* **1937**, 1468.

(72) Stetter, H.; Mayer, K.-H. *Chem. Ber.* **1961**, *94*, 1410–1416.
(73) Stetter, H.; Roos, E.-E. *Chem. Ber.* **1954**, *87*, 566–571.
(74) Richman, J. E.; Atkins, T. J. *J. Am. Chem. Soc.* **1974**, *96*, 2268–2270.
(75) Vriesema, B. K.; Buter, J.; Kellogg, R. M. *J. Org. Chem.* **1984**, *49*, 110–113.
(76) Senboku, H.; Nakahara, K.; Fukuhara, T.; Hara, S. *Tetrahedron Lett.* **2010**, *51*, 435–438.
(77) Wieghardt, K.; Chaudhuri, P.; Nuber, B.; Weiss, J. *Inorg. Chem.* **1982**, *21*, 3086–3090.
(78) Weisman, G. R.; Vachon, D. J.; Johnson, V. B.; Gronbeck, D. A. *J. Chem. Soc. Chem. Commun.* **1987**, 886.
(79) Sessler, J. L.; Sibert, J. W.; Lynch, V. *Inorg. Chem.* **1990**, *29*, 4143–4146.
(80) Chong, H.; Brechbiel, M. W. *Synth. Commun.* **2003**, *33*, 1147–1154.
(81) Romakh, V. B.; Therrien, B.; Süss-Fink, G.; Shul'pin, G. B. *Inorg. Chem.* **2007**, *46*, 1315–1331.
(82) Belousoff, M. J.; Duriska, M. B.; Graham, B.; Batten, S. R.; Moubaraki, B.; Murray, K. S.; Spiccia, L. *Inorg. Chem.* **2006**, *45*, 3746–3755.
(83) Silver, G. C.; Trogler, W. C. *J. Am. Chem. Soc.* **1995**, *117*, 3983–3993.
(84) Schoenfeldt, N. J.; Ni, Z.; Korinda, A. W.; Meyer, R. J.; Notestein, J. M. *J. Am. Chem. Soc.* **2011**, *133*, 18684–18695.
(85) Huang, J.; Zhou, Z.; Chan, T. *Synthesis* **2009**, *2009*, 2341–2344.
(86) Chong, H.; Garmestani, K.; Ma, D.; Milenic, D. E.; Overstreet, T.; Brechbiel, M. W. *J. Med. Chem.* **2002**, *45*, 3458–3464.
(87) Meca, L.; Císařová, I.; Dvořák, D. *Organometallics* **2003**, *22*, 3703–3709.
(88) Wieghardt, K. *Pure Appl. Chem.* **1988**, *60*.
(89) DeRonde, M.; Driscoll, D.; Yang, R.; Zompa, L. J. *Inorg. Nucl. Chem. Lett.* **1975**, *11*, 521–523.
(90) Koyama, H.; Yoshino, T. *Bull. Chem. Soc. Jpn.* **1972**, *45*, 481–484.
(91) Belousoff, M. J.; Graham, B.; Moubaraki, B.; Murray, K. S.; Spiccia, L. *Eur. J. Inorg. Chem.* **2006**, *2006*, 4872–4878.
(92) Chaudhuri, P.; Ventur, D.; Wieghardt, K.; Peters, E.-M.; Peters, K.; Simon, A. *Angew. Chem.* **1985**, *97*, 55–56.
(93) Zhang, Z.; Shao, D.-L.; Geng, Z.-R.; Wang, Z.-L. *Z. Für Anorg. Allg. Chem.* **2012**, *638*, 821–825.
(94) Housecroft, C. E.; Sharpe. *Inorganic chemistry*; Pearson Prentice Hall: Harlow, England; New York, 2008.
(95) *IUPAC Compendium of Chemical Terminology: Gold Book*; Nič, M.; Jirát, J.; Košata, B.; Jenkins, A.; McNaught, A., Eds.; 2.1.0 ed.; IUPAC: Research Triagle Park, NC, 2009.
(96) *Kirk-Othmer Encyclopedia of Chemical Technology*; John Wiley & Sons, Inc., Ed.; John Wiley & Sons, Inc.: Hoboken, NJ, USA, 2000.
(97) Jurinke, C.; Oeth, P.; van den Boom, D. *Mol. Biotechnol.* **2004**, *26*, 147–164.
(98) Neurath, H. *Science* **1984**, *224*, 350–357.
(99) Hegg, E. L.; Burstyn, J. N. *J. Am. Chem. Soc.* **1995**, *117*, 7015–7016.
(100) *Organic chemistry*; Clayden, J., Ed.; Oxford University Press: Oxford ; New York, 2001.
(101) Pocker, Y.; Stone, J. T. *Biochemistry (Mosc.)* **1967**, *6*, 668–678.
(102) Kirby, A. J.; Jencks, W. P. *J. Am. Chem. Soc.* **1965**, *87*, 3209–3216.
(103) Lee, C. K.; Diesendruck, C. E.; Lu, E.; Pickett, A. N.; May, P. A.; Moore, J. S.; Braun, P. V. *Macromolecules* **2014**, *47*, 2690–2694.
(104) Mabilleau, G.; Stancu, I. C.; Honoré, T.; Legeay, G.; Cincu, C.; Baslé, M. F.; Chappard, D. *J. Biomed. Mater. Res. A* **2006**, *77A*, 35–42.
(105) Jakobs, RTM (Bob). Catalysis and luminescence in mechanically activated polymers, 2013.

# Appendix A

$^{1}$H-NMR spectrum compound **12**

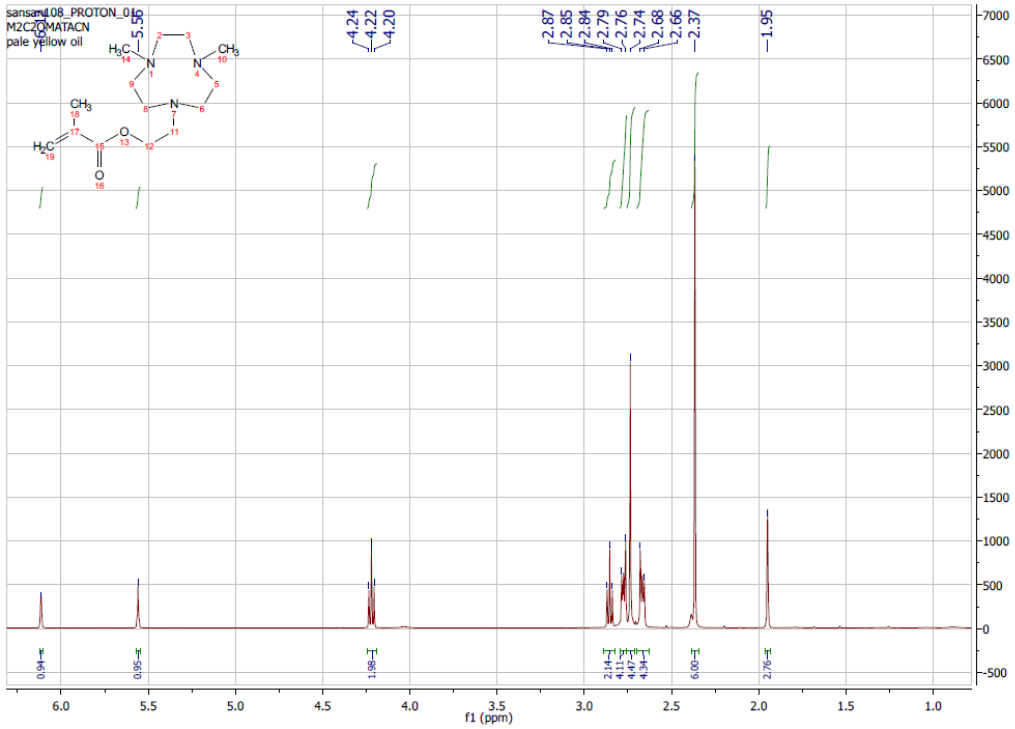


$^{1}$H-NMR spectrum compound **13**

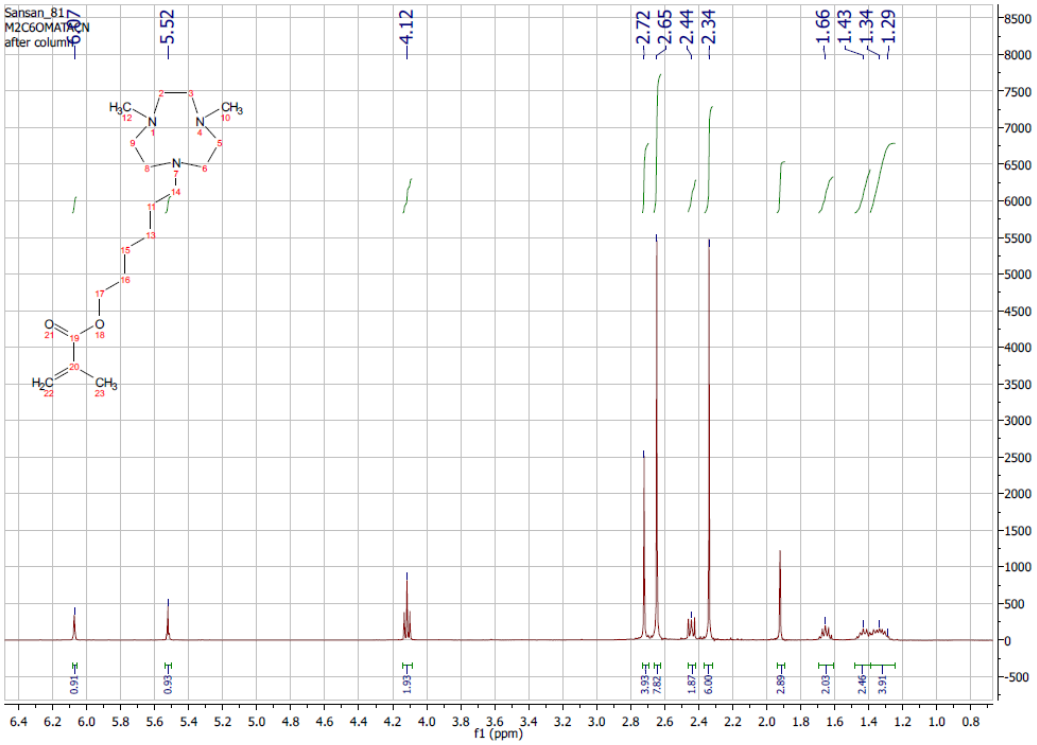

## Appendix B

Maldi-TOF MS of compound **12**

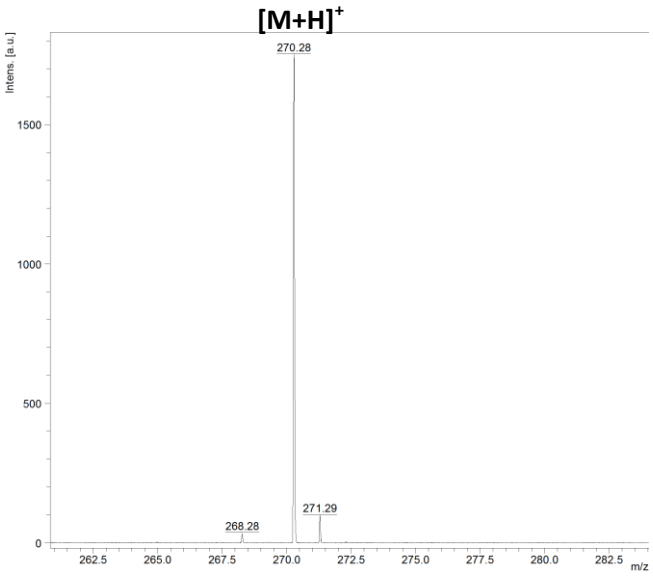


Maldi-TOF MS (zoom in) of complex **[L2Cu-μ-Ox]**

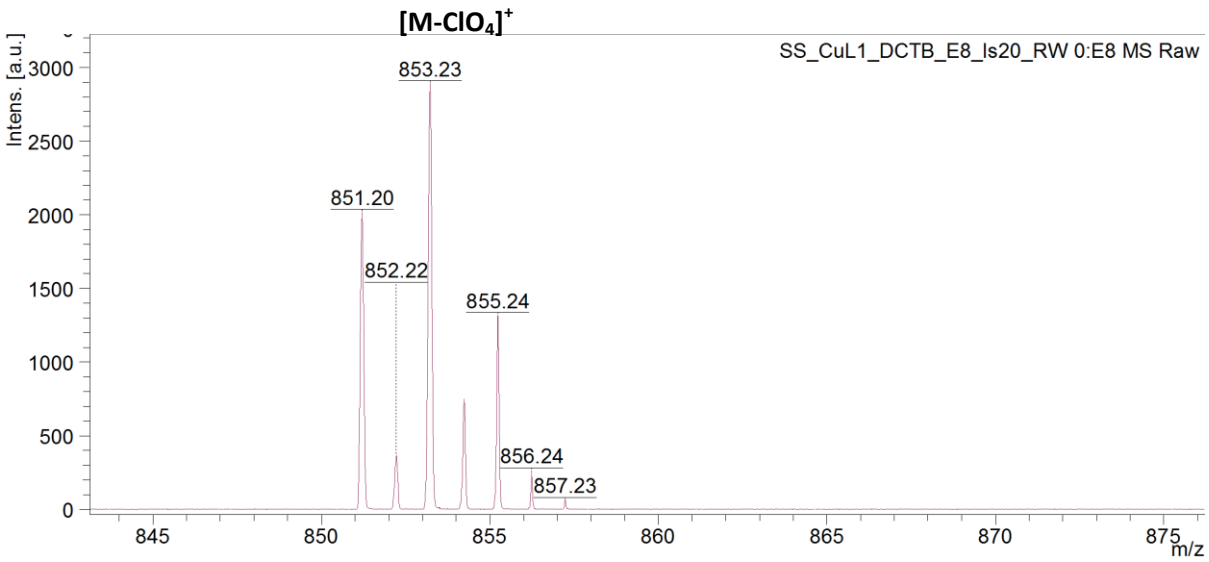

# Appendix C

IR spectrum of compound **12**

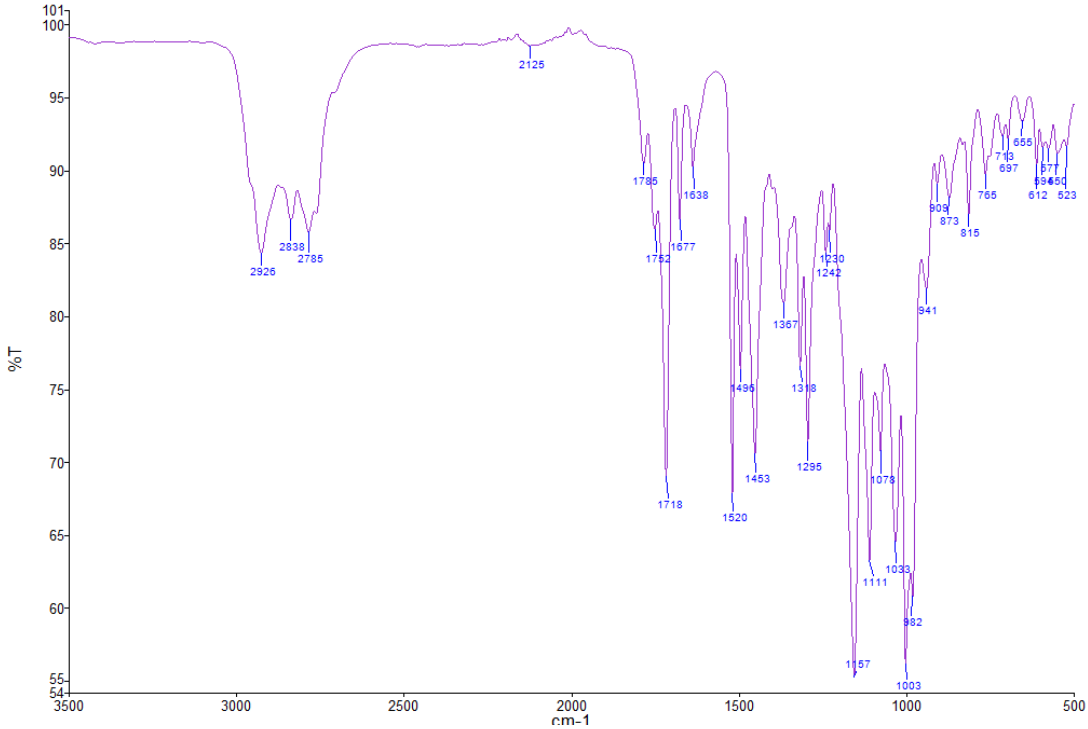


IR spectrum of complex **[L2Cu-μ-Ox]**

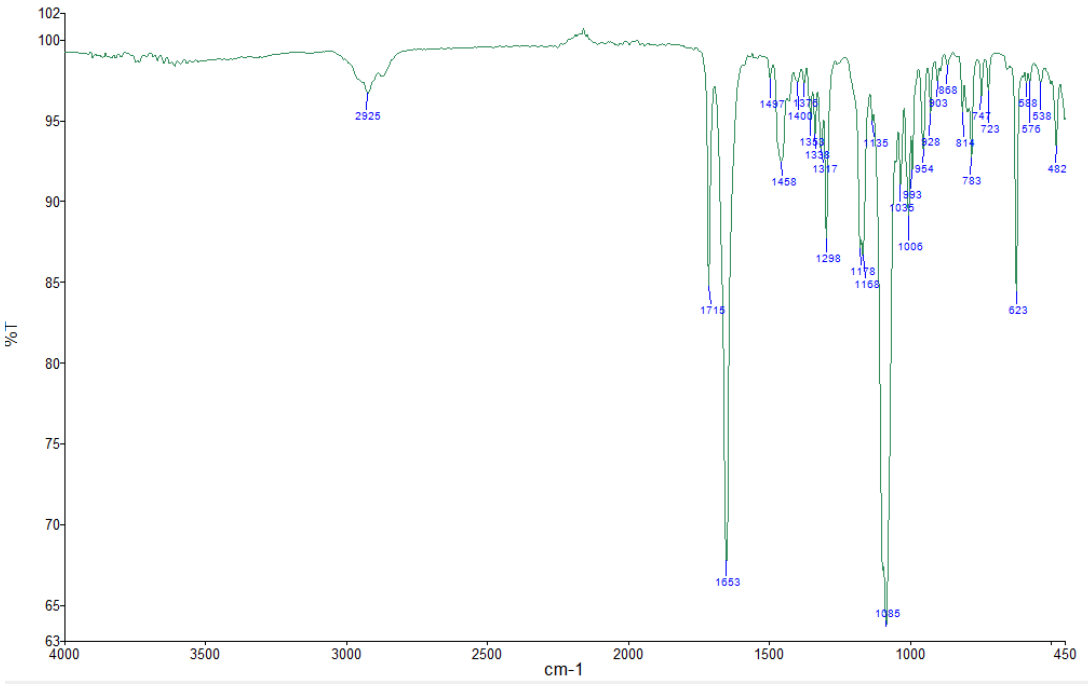

IR spectrum of complex **[L3Cu-μ-Ox]**

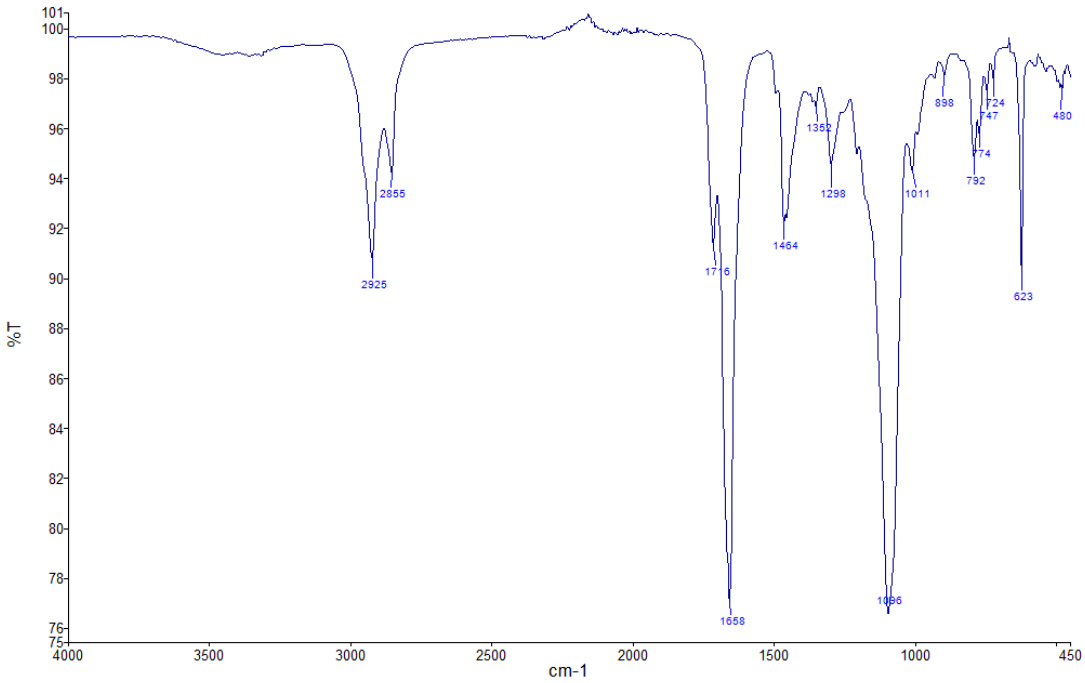

# Appendix D

Preparation of buffer solutions:

**Table D.1 Used amounts in the preparation of buffers**

| Buffer | pH7A | pH9A | pH7B | pH9B |
|---|---|---|---|---|
| | MOPS | CHES | MOPS | CHES |
| pH | 7 | 8,8 | 7 | 8,8 |
| concentration buffer (M) | 0,1 | 0,1 | 0,05 | 0,05 |
| Ionic strength (M) | 0,3 | 0,3 | 0,15 | 0,15 |
| g buffer | 2,09 | 1,04 | 1,05 | 1,04 |
| g NaClO4 | 3,17 | 3,17 | 1,59 | 1,59 |
| mL water | 100 | 100 | 100 | 100 |

The buffer solutions were prepared at room temperature, MOPS or CHES (Table D.1) was dissolved in around $H_2O$ (70 ml) , and $NaClO_4$ (Table D.1) was added. The pH of this solution was measured. This was adjusted to the desired pH upon addition of 2M NaOH. The remaining $H_2O$ was added to volume of 100 mL. The pH was measured again.

# Appendix E

**Table E. 1 Preparation of solution for polymerization of films**

| Film | wt% initiator | mol% TEGDA | mol% [L2Cu-μ-Ox] | mL stock TEGDA (10 mg/mL) | mL stock initiator (10 mg/mL) | mL[L2Cu-μ-Ox] stock (5 mg/mL) | mL HEMA |
|---|---|---|---|---|---|---|---|
| **pHEMA-Cu4** | 0,1 | 0,99 | 0,01 | 0,49 | 0,03 | 0,03 | 0.2 |
| **pHEMA-Cu5** | 0,1 | 0,95 | 0,05 | 0,47 | 0,03 | 0,15 | 0.2 |
| **pHEMA-Cu6** | 0,5 | 0,99 | 0,01 | 0,49 | 0,11 | 0,03 | 0.2 |
| **pHEMA-Cu7** | 0,5 | 0,95 | 0,05 | 0,47 | 0,11 | 0,15 | 0.2 |
| **pHEMA-control2** | 0,1 | 1 | 0 | 0,5 | 0,03 | 0 | 0.2 |
| **pHEMA-control3** | 0,5 | 1 | 0 | 0,5 | 0,11 | 0 | 0.2 |

**Table E. 2 Preparation of solutions in swelling studies**

| Film | mg polymer | mL BNPP (from stock (10 mM)) | mL Buffer pH9A | mL water |
|---|---|---|---|---|
| **pHEMA-Cu4** | 16,6 | 0,248 | 1,244 | 0,995 |
| **pHEMA-Cu5** | 8,2 | 0,384 | 1,92 | 1,536 |
| **pHEMA-Cu6** | 20 | 0,289 | 1,448 | 1,158 |
| **pHEMA-Cu7** | 5,4 | 0,447 | 2,235 | 1,788 |
| **pHEMA-control2** | 26,8 | 0,3 | 1,5 | 1,2 |
| **pHEMA-control3** | 22,2 | 0,3 | 1,5 | 1,2 |